The ancestral retinoic acid receptor was a low-affinity sensor triggering neuronal differentiation

Mette Handberg-Thorsager, Juliana Gutierrez-Mazariegos, Stefan T. Arold, Eswar Kumar Nadendla, Paola y Bertucci, Pierre Germain, Pavel Tomançak, Keely Pierzchalski, Jace W Jones, Ricard Albalat, et al.

DEVELOPMENTAL BIOLOGY

The ancestral retinoic acid receptor was a low-affinity sensor triggering neuronal differentiation

Mette Handberg-Thorsager,[1]*† Juliana Gutierrez-Mazariegos,[2]† Stefan T. Arold,[3] Eswar Kumar Nadendla,[4] Paola Y. Bertucci,[1] Pierre Germain,[4] Pavel Tomančak,[5] Keely Pierzchalski,[6] Jace W. Jones,[6] Ricard Albalat,[7] Maureen A. Kane,[6] William Bourguet,[4] Vincent Laudet,[2‡§¶] Detlev Arendt,[1,8‡¶] Michael Schubert[9‡¶]

Retinoic acid (RA) is an important intercellular signaling molecule in vertebrate development, with a well-established role in the regulation of *hox* genes during hindbrain patterning and in neurogenesis. However, the evolutionary origin of the RA signaling pathway remains elusive. To elucidate the evolution of the RA signaling system, we characterized RA metabolism and signaling in the marine annelid *Platynereis dumerilii*, a powerful model for evolution, development, and neurobiology. Binding assays and crystal structure analyses show that the annelid retinoic acid receptor (RAR) binds RA and activates transcription just as vertebrate RARs, yet with a different ligand-binding pocket and lower binding affinity, suggesting a permissive rather than instructive role of RA signaling. RAR knockdown and RA treatment of swimming annelid larvae further reveal that the RA signal is locally received in the medial neuroectoderm, where it controls neurogenesis and axon outgrowth, whereas the spatial colinear *hox* gene expression in the neuroectoderm remains unaffected. These findings suggest that one early role of the new RAR in bilaterian evolution was to control the spatially restricted onset of motor and interneuron differentiation in the developing ventral nerve cord and to indicate that the regulation of *hox*-controlled anterior-posterior patterning arose only at the base of the chordates, concomitant with a high-affinity RAR needed for the interpretation of a complex RA gradient.

INTRODUCTION

In vertebrates, retinoic acid (RA) regulates a wide range of biological processes in development and adult life. During embryogenesis, RA controls patterning along the anteroposterior body axis and is required for the proper formation of various organs, including heart, liver, kidney, limbs, and the nervous system (*1*, *2*). In the developing central nervous system, RA mediates anteroposterior regionalization via the direct control of *hox* transcription and subsequently stimulates neurogenesis and promotes neuronal differentiation via the activation of *pax6*, *ngn2*, and *dbx1* in specific regions of the neuroectoderm (*1*, *2*).

In vivo, RA is synthesized from vitamin A in two different oxidative steps. The first one, the rate-limiting dehydrogenation of retinol to retinal, is catalyzed by retinol dehydrogenases (RDHs) of the short- or medium-chain dehydrogenase/reductase superfamilies [for example, SDR-RDH10 or MDR-ADH3 (alcohol dehydrogenase 3)] (*3*). Alternatively, retinal can be further produced from the enzymatic cleavage of β-carotene by carotenoid cleavage oxygenase (CCO) enzymes. The second step, the production of RA from retinal, is catalyzed by the retinaldehyde dehydrogenases (RALDHs). Although different isomers of RA exist, such as all-*trans* RA (ATRA), 9-*cis* RA (9cRA), and 13-*cis* RA (13cRA), the most important biologically active RA isomer in vertebrates is ATRA (*3*, *4*).

The major mediators of RA signaling are the retinoic acid receptor (RAR) and the retinoid X receptor (RXR), which are ligand-dependent transcription factors belonging to the nuclear receptor superfamily. RAR and RXR heterodimerize on specific DNA stretches, called RA response elements (RAREs), present in the promoter regions of target genes (*5*–*7*). The RAR ligand-binding domain (LBD) mediates the high-affinity binding of ATRA with a dissociation constant in the nanomolar range (K_d = 0.4 nM) (*8*). The LBD contains 12 helices that form the ligand-binding pocket (LBP) (*9*), and binding of the ligand modifies the position of helix 12, allowing the recruitment of coactivators. This association of coactivators, in turn, leads to the initiation of transcription of RA target genes (*7*, *10*, *11*).

Although RA signaling is traditionally described as a chordate innovation, key elements of the RA machinery, such as RAR and RXR, have been identified in several nonchordate genomes (*12*, *13*). For example, genes encoding RAR, RXR, and RALDH, as well as the RA-catabolizing enzyme CYP26 (cytochrome P450 subfamily 26), have been identified in the annelid *Capitella teleta* (*12*, *13*). In contrast, in the annelid *Helobdella robusta*, RAR and CYP26 have been lost (*13*), and the only report of roles of RA in annelids assessed the effects of very high concentrations of retinal on juvenile and regenerating worms (*14*).

[1]Developmental Biology Unit, European Molecular Biology Laboratory, Meyerhofstrasse 1, 69012 Heidelberg, Germany. [2]Molecular Zoology Team, Institut de Génomique Fonctionnelle de Lyon, Université de Lyon, Université Lyon 1, CNRS, Institut National de la Recherche Agronomique, Ecole Normale Supérieure de Lyon, 46 Allée d'Italie, 69364 Lyon Cedex 07, France. [3]King Abdullah University of Science and Technology, Center for Computational Bioscience Research, Division of Biological and Environmental Sciences and Engineering, Thuwal 23955-6900, Saudi Arabia. [4]Centre de Biochimie Structurale, Inserm, CNRS, Université de Montpellier, 29 Rue de Navacelles, 34090 Montpellier, France. [5]Max Planck Institute of Molecular Cell Biology and Genetics, Pfotenhauerstrasse 108, 01307 Dresden, Germany. [6]Department of Pharmaceutical Sciences, School of Pharmacy, University of Maryland, 20 North Pine Street, Baltimore, MD 21201, USA. [7]Departament de Genètica, Microbiologia i Estadística, Institut de Recerca de la Biodiversitat (IRBio), Facultat de Biologia, Universitat de Barcelona, Avinguda Diagonal 643, 08028 Barcelona, Spain. [8]Centre for Organismal Studies, University of Heidelberg, Im Neuenheimer Feld 230, 69120 Heidelberg, Germany. [9]Sorbonne Universités, Université Pierre et Marie Curie (UPMC) Université Paris 06, CNRS, Laboratoire de Biologie du Développement de Villefranche-sur-Mer, Observatoire Océanologique de Villefranche-sur-Mer, 181 Chemin du Lazaret, 06230 Villefranche-sur-Mer, France.
*Present address: Max Planck Institute of Molecular Cell Biology and Genetics, Pfotenhauerstrasse 108, 01307 Dresden, Germany.
†These authors contributed equally to this work.
‡These authors contributed equally to this work.
§Present address: Sorbonne Universités, Université Pierre et Marie Curie (UPMC) Université Paris 06, CNRS, Observatoire Océanologique de Banyuls-sur-Mer, Avenue Pierre Fabre, 66650 Banyuls-sur-Mer, France.
¶Corresponding author. Email: michael.schubert@obs-vlfr.fr (M.S.); arendt@embl.de (D.A.); vincent.laudet@obs-banyuls.fr (V.L.)

Furthermore, the functional characterization of RARs from two gastropod mollusks, *Thais clavigera* and *Nucella lapillus*, has established that these receptors are unable to bind RA (*15*, *16*). Therefore, albeit the presence of the main RA signaling components in various bilaterian taxa, RAR-dependent RA signaling still retains its status as a chordate-specific feature.

Here, we describe the characterization of a novel RAR cloned from the annelid *Platynereis dumerilii*. We show that the *P. dumerilii* RAR (PduRAR) acts as ligand-activated transcription factor in the presence of ATRA and 13cRA, both of which are present in embryos, larvae, and adults. However, RA activates the annelid receptor only in the micromolar range, indicating that PduRAR is a low-affinity RA sensor and not a chordate-type high-affinity RAR. Furthermore, the crystal structure of the PduRAR LBD reveals that differential binding of RA molecules to the LBPs of the *P. dumerilii* and vertebrate receptors defines the structural basis for these affinity differences. During development, PduRAR does not control anteroposterior patterning of the embryo and does not regulate *hox* gene expression. In contrast, RA signaling functions during annelid neurogenesis to control differentiation and axonal outgrowth of medial neuron types in the ventral nerve cord. Our work is the first to unravel RAR function outside chordates and suggests that one early role of RAR-dependent RA signaling was the spatiotemporal control of motor and interneuron differentiation. Our comparative data indicate that the ancestral RAR likely acted as a permissive sensor and that high-affinity, instructive RARs evolved only at the base of chordates, concomitant with a role for RA signaling in global anteroposterior patterning through *hox* gene regulation.

RESULTS

Identification of RA signaling pathway components in *P. dumerilii*

To gain insights into the evolution of the RA pathway, we screened transcriptomic and genomic databases of the marine annelid *P. dumerilii* (*17*) for molecular components characterizing chordate RA signaling (*3*). These included genes encoding the nuclear receptors RAR and RXR, enzymes involved in RA synthesis and degradation [CCO, SDR, MDR, RALDH—that is, members of the aldehyde dehydrogenase 1a (ALDH1a) and ALDH8a subfamilies—and CYP26], retinoid transport proteins and plasma membrane–associated receptors [cellular RA-binding protein (CRABP), cellular retinol-binding protein (CRBP), retinol-binding protein 4 (RBP4), transthyretin (TTR), and stimulated by RA 6 (STRA6)], and enzymes involved in the synthesis and degradation of retinoid storage products [lecithin-retinol acyltransferase (LRAT), acyl-CoA:retinol acyltransferase (DGAT), and retinoid isomerohydrolase (RPE65)] (Fig. 1).

Phylogenetic analyses of the obtained gene sequences allowed us to identify single *rar* and *rxr* homologs in *P. dumerilii.* Furthermore, we characterized five *aldh1a*, one *aldh8a*, three *cyp26*, one *sdr-rdh10*, one *mdr-adh3*, and three *cco* genes, demonstrating that the basic RA signaling machinery, composed of receptors as well as RA-synthesizing and RA-degrading enzymes, is present in *P. dumerilii* (Fig. 1 and fig. S1). A vertebrate-type RA metabolism and RAR-dependent signaling were thus already present at the base of bilaterians.

To maintain retinoid homeostasis, vertebrates can accumulate retinoids in the liver and mobilize them to satisfy the RA requirements of peripheral tissues. Retinol is esterified to retinyl esters by the action of the vertebrate LRAT or DGAT1 enzymes, and retinyl esters can be transformed back to retinol by retinyl ester hydrolases (including RPE65) (*18*). *P. dumerilii* seems to lack *lrat* and *rpe65* orthologs, although an ortholog of *dgat* has been identified in *P. dumerilii*, suggesting that de novo synthesis of retinyl esters is possible (Fig. 1 and fig. S1).

Retinoids are generally bound to proteins that solubilize and stabilize them in aqueous environments. *P. dumerilii* lacks homologs of the typical vertebrate retinoid binding proteins, that is, of the intracellular *crbp* and *crabp*, as well as of the extracellular *rbp4* and *ttr*. Concomitantly, *stra6*, the membrane receptor required for *rbp4*-dependent retinol uptake into target cells in vertebrates (*3*), is also absent from *P. dumerilii*. These data suggest that, although the core components of the RA

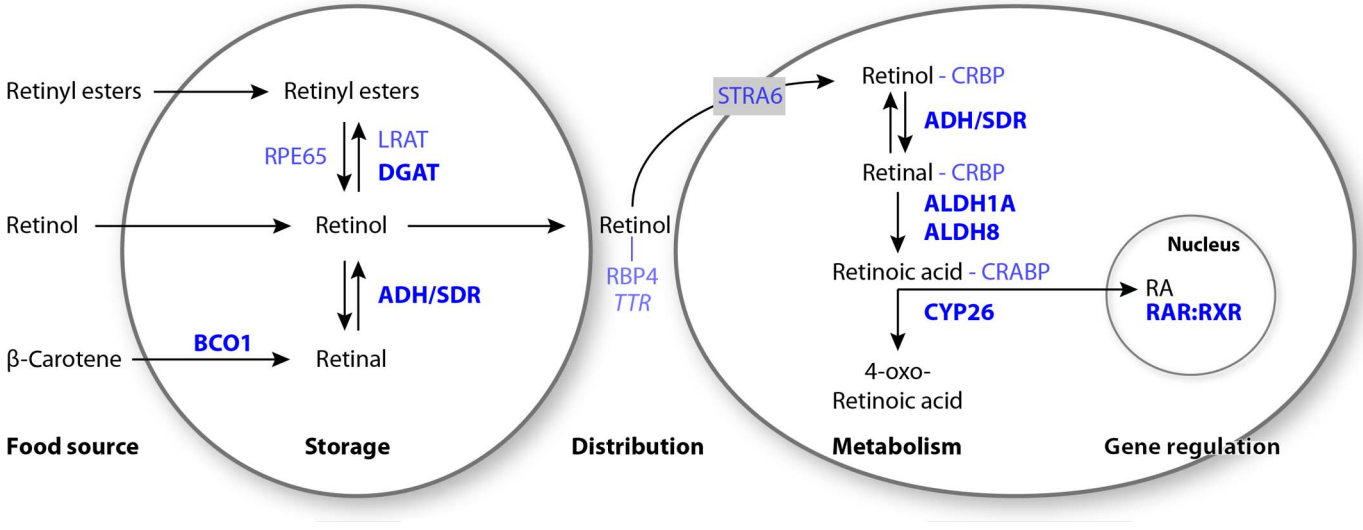

Fig. 1. Molecular components of retinoid metabolism and signaling. Schematic representation of retinoid metabolism, storage, transport, and signaling in vertebrates. Metabolic enzymes, binding proteins, and nuclear receptors are shown in blue. Names in bold letters indicate the presence of a gene encoding the ortholog of a given vertebrate protein in the *P. dumerilii* genome. Italic lettering indicates the absence of the complete corresponding gene family in *P. dumerilii*. Names in regular letters indicate the presence, in *P. dumerilii*, of members of a given gene family but the absence of a specific *P. dumerilii* ortholog of the corresponding vertebrate gene. Of note, the involvement of ADH enzymes in retinal synthesis in vertebrates has been challenged (*3*).

pathway are conserved between *P. dumerilii* and vertebrates (that is, ligand production/degradation and receptors), key mechanisms for retinoid storage, intercellular transport, cellular uptake, and intracellular binding of retinoids are not. This is consistent with the idea that the vertebrate components for hepatic storage, mobilization, and transport of retinoids were lineage-specific innovations (*18*).

Molecular characterization of the PduRAR

To characterize the PduRAR and PduRXR proteins in vitro, we cloned and expressed the respective genes. The DNA binding domain of the annelid RAR shares approximately 88% sequence identity with that of the three human RARs (RARα, RARβ, and RARγ) and 92% with that of a recently identified mollusk RAR (*N. lapillus*) (*16*). In contrast, the LBD shares only about 55% identity with that of the human RARs and 60% with that of the *N. lapillus* RAR, and of the 25 amino acids known to interact with ATRA in the LBP of the human RARα (*19*), 5 are different in the annelid ortholog (fig. S2).

The DNA binding properties of the annelid RAR/RXR heterodimer were validated using electrophoretic mobility shift assays (EMSAs) (Fig. 2A). Binding was assessed on consensus direct repeat (DR) elements as defined for vertebrates (*8*). Using a radiolabeled DR2 probe, no binding of RAR or RXR alone could be detected. In contrast, the RAR/RXR heterodimer strongly bound the DR2 element. This binding was specific because it was outcompeted by an excess of unlabeled DR2 probe but not by a nonspecific unlabeled probe. Binding was also lost in the presence of unlabeled DR1 and DR5. Other elements, such as DR0, DR3, and DR4, induced only marginal competition. These results indicate that the annelid RAR/RXR heterodimer binds specifically to a range of RAREs very similar to those of its vertebrate orthologs (that is, DR1, DR2, and DR5).

We subsequently tested the ability of the PduRAR to bind different retinoids and activate transcription in a ligand-dependent manner. First, we performed transient transactivation assays using a Gal4 LBD receptor chimera. Our results show that the RAR LBD is able to activate transcription of a luciferase reporter gene in a dose-dependent manner in the presence of ATRA, 13cRA, and 9cRA, with ATRA and 13cRA eliciting a stronger response than 9cRA (Fig. 2B). However, it is important to note that for any of the three ligands, an activation of the receptor was observed only with relatively high ligand concentrations (1 to 10 μM). This is in stark contrast to the situation in vertebrates, where RAR activation by ATRA is already observed at a concentration of 1 nM (*20*).

Direct binding analyses of PduRAR to different ligands using limited proteolysis assays (LPAs) confirmed these results (Fig. 2C). We observed that, starting at a concentration of 1 μM, the RAR LBD was protected from proteolysis by all three ligands. The specificity of these effects was validated using the RAR antagonist BMS493 (*21*). In the presence of ATRA, high concentrations of BMS493 (10 μM) induced a decrease in the transcription of the luciferase reporter gene (Fig. 2D). Furthermore, LPAs showed a BMS493-induced protection from proteolysis starting at a concentration of 1 μM, indicating that BMS493 binding to the LBD antagonized the ATRA-dependent transcriptional activity of RAR (Fig. 2E). Of note, the annelid RXR activated transcription of a luciferase reporter gene in a concentration-dependent manner using either 9cRA or the RXR-specific agonist BMS649 (fig. S3A) (*22*). Moreover, the use of the RXR-specific antagonist UVI3003 (*23*) inhibited RXR transcriptional activity (fig. S3B).

After the characterization of the ligand-binding properties, we assessed the capacity of the annelid RAR to interact with receptor cofactors,

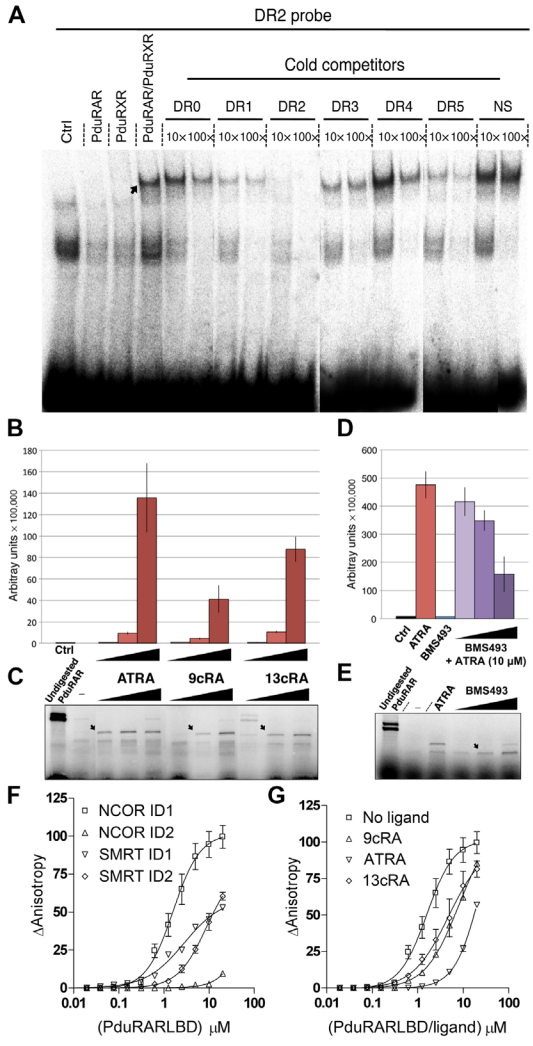

Fig. 2. Molecular characterization of PduRAR. (**A**) DNA recognition by the PduRAR/PduRXR heterodimer. Both receptors were synthesized in vitro, and the heterodimer was allowed to bind to a ^{32}P-labeled DR2 RARE probe. Cold competitors correspond to 10- or 100-fold excess of unlabeled oligonucleotides (DR0 to DR5). A nonspecific element (NS) was used as a negative control. Unprogrammed reticulocytes were used as control (Ctrl). Protein and labeled probe complexes are indicated by an arrow (shown only in the PduRAR/PduRXR lane). (**B**) The ability of PduRAR to activate the transcription of the luciferase reporter gene was tested in transfected human embryonic kidney (HEK) 293T cells in the presence of increasing concentrations (0.1, 1, and 10 μM) of ATRA, 9cRA, and 13cRA. The Gal4 DNA binding domain construct alone was used as a negative control (Ctrl). Bars are means ± SD (n = 3). (**C**) The ability of PduRAR to bind different ligands was tested by LPA. The ligands (ATRA, 9cRA, and 13cRA) were used at increasing concentrations (0.1, 1, and 10 μM). Ethanol was used as a negative control (lane –), and protected bands are indicated by arrows. (**D**) Competition assay using increasing concentrations of the RAR antagonist BMS493 (0.1, 1, and 10 μM) in the presence of 10 μM ATRA. The Gal4 DNA binding domain construct alone was used as a negative control (Ctrl). Bars are means ± SD (n = 3). (**E**) Binding of PduRAR to increasing concentrations of BMS493 (0.1, 1, and 10 μM) as assessed by LPA. Ethanol was used as a negative control (lane –), and protected bands are indicated by arrows. (**F**) Titration of the fluorescein-labeled interaction domains (ID1 and ID2) of the corepressors NCOR (nuclear receptor corepressor) and SMRT (silencing mediator for retinoid and thyroid hormone receptors) by unliganded PduRAR monitored by fluorescence anisotropy. Assays were performed in three independent experiments, and data are expressed as means ± SEM. (**G**) Titration of the fluorescein-labeled interaction domain 1 (ID1) of the corepressor NCOR by PduRAR in the presence of different retinoids: ATRA, 9cRA, and 13cRA. Assays were performed in three independent experiments, and data are expressed as means ± SEM.

using a fluorescence-based assay that monitors the ligand-induced association of cofactor fragments. Two corepressors, NCOR (nuclear receptor corepressor) and SMRT (silencing mediator for retinoid and thyroid hormone receptor), were analyzed because they are known to interact with unliganded vertebrate receptors through two interaction domains (called ID1 and ID2) (*24*). Using fluorescein-labeled peptides derived from NCOR and SMRT, we first evaluated the binding preferences of RAR in the absence of ligand. We found that RAR bound most avidly to NCOR ID1 (Fig. 2F). We then titrated the NCOR ID1 peptide with RAR in the presence of different retinoids (ATRA, 13cRA, and 9cRA) (Fig. 2G). As expected, we observed that the three retinoids are able to bind to RAR and induce NCOR ID1 release, with ATRA being more potent than 13cRA and 9cRA in inducing the dissociation (Fig. 2G).

To gain insights into the molecular mechanisms of annelid RAR ligand binding, we determined the crystal structure of the LBD of the PduRAR in complex with ATRA at a resolution of 2.7 Å (table S1). The asymmetric unit contained four molecules organized as two LBD homodimers (fig. S4A). Electron density for the ligand was only visible in subunits B and D, each of which formed dimers with a nonliganded LBD (subunits A and C, respectively) (fig. S4, A and B). All four subunits superimposed very well, except in the N-terminal region of helix H3 and the C-terminal part of the domain containing helix H11 and the activation helix H12 (Fig. 3A). In molecules B and D, the N termini of helix H3 and helix H11 were shifted outward of the LBP to accommodate the ATRA molecule. Unexpectedly, helices H12 of the ligand-bound molecules B and D were not stabilized in the so-called agonist-bound or active conformation but docked onto the surface of a symmetry-related liganded LBD, resulting in an arm-exchanged conformation (Fig. 3A and fig. S4C). We were unable to observe any interpretable electron density for the ligand in molecules A and C, whose helices H12 were in the agonist- and antagonist-bound conformations, respectively (Fig. 3A). Both subunits B and D bound ATRA in an orientation that has never been observed in mammalian RAR structures (Fig. 3B). Although molecules B and D were involved in different crystal packing interactions, their ATRA molecules were fully superimposable, strongly supporting the fact that the unusual binding mode of the ligand was not influenced by crystal packing constraints.

In human RARα, the LBP extends from helix H11 on one side to the two conserved polar residues R276 in helix H5 and S287 in the tip of the β-turn S1/S2, which form a hydrogen bond network with the carboxylate moiety of the retinoid ligand on the other side (Fig. 3B). In contrast, in the PduRAR, the ligand is rotated by almost 90°, resulting in the carboxyl group of ATRA lying between the N-terminal region of helices

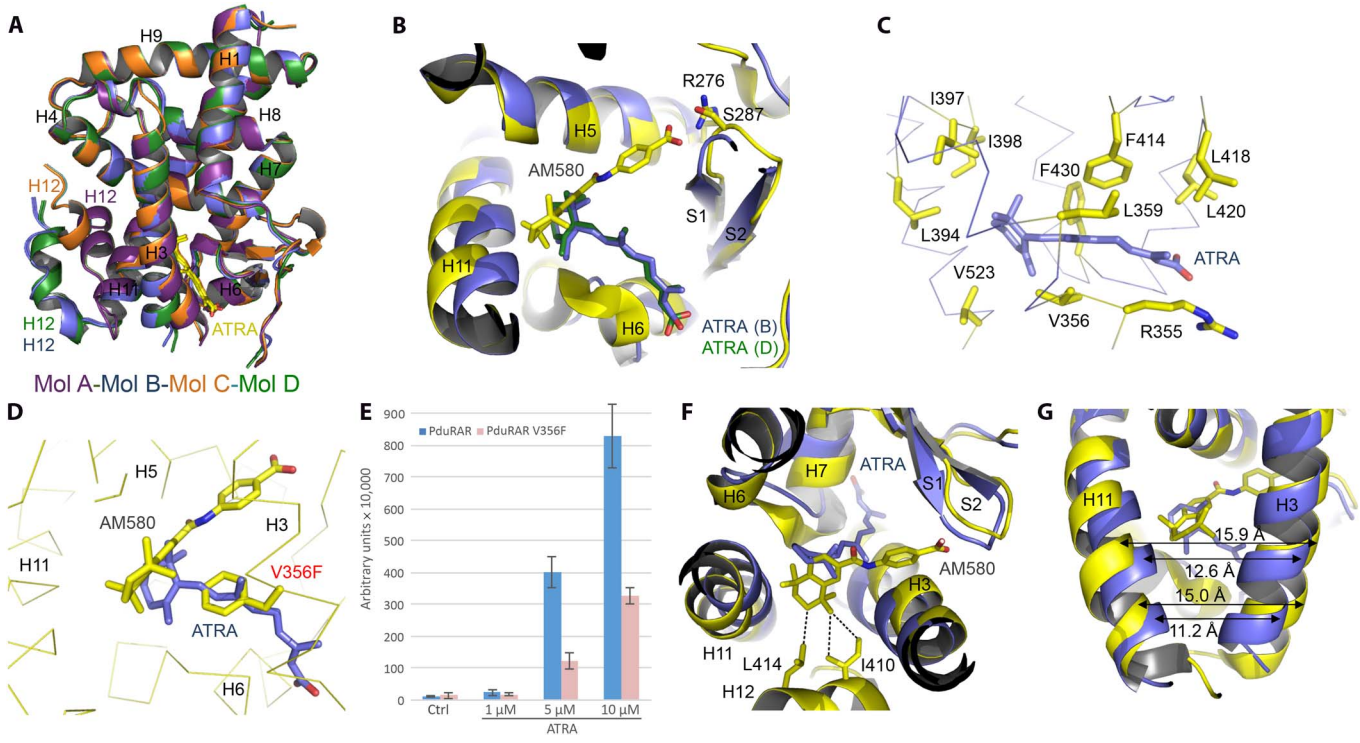

Fig. 3. Crystal structure of the PduRAR LBD. (**A**) Superimposition of the four PduRAR LBDs (Mol A to Mol D) contained in the asymmetric unit. α Helices (H1 to H12) are labeled. The two ATRA molecules present in subunits B and D are shown as yellow sticks. (**B**) Superimposition of the LBPs of human RARα bound to the agonist AM580 (yellow) and of the PduRAR (Mol B) bound to ATRA (blue). The ATRA present in Mol D (which was superimposed on Mol B and is not shown) is displayed as green sticks. Human RARα R276 and S287 that are engaged in polar interactions with the carboxylate moiety of AM580 are shown. (**C**) Close-up view of the LBP of PduRAR bound to ATRA. Residues in contact with the ligand are shown and labeled. (**D**) Superimposition of the LBPs of human RARα bound to the agonist AM580 (yellow) and of the PduRAR (Mol B) bound to ATRA (blue) showing how the V356F mutation affects ligand binding to the annelid receptor. (**E**) Transcriptional activity of the PduRAR V356F mutant, in transfected HEK 293T cells, in the presence of increasing concentrations of ATRA (1, 5, and 10 μM). The GAL4 DNA binding domain alone was used as a negative control (Ctrl). Bars are means ± SD (n = 3). (**F**) Superimposition of the LBPs of human RARα bound to the agonist AM580 (yellow) and of the PduRAR (Mol B) bound to ATRA (blue). The van der Waals interactions between AM580 and helix H12 residues I410 and L414 are indicated as dotted lines. (**G**) Superimposition of the LBPs of human RARα bound to the agonist AM580 (yellow) and of the PduRAR (Mol B) bound to ATRA (blue), highlighting the smaller distances between equivalent residue positions in helices H3 and H11 in the annelid receptor when compared to vertebrate receptors.

H3 and H6 (Fig. 3, A and B). The vast majority of the contacts made by ATRA with the LBP were loose van der Waals interactions, and the carboxylate moiety of the ligand did not form any noticeable hydrogen bonds with surrounding LBP residues (Fig. 3C). This structure suggested that the carboxylate moiety plays little role in the binding of retinoids to PduRAR, which strongly contrasts the situation in human RARs. This observation was in agreement with our cell-based results showing similar binding efficiencies of ATRA, 13cRA, and 9cRA for the annelid receptor (Fig. 2B). To validate the alternative binding mode of PduRAR, we mutated the valine at position 356 in helix H3 into a phenylalanine (V356F), which is the corresponding residue at this position in human RARs (F228 in RARα) (Fig. 3D). On the basis of the structure, this substitution should specifically affect the PduRAR binding mode. In agreement with this hypothesis, we observed a marked decrease in the capacity of ATRA to activate the V356F mutant (Fig. 3E).

Comparisons of the ATRA-bound PduRAR LBD structure to that of the human RARα LBD bound to the agonist AM580 (*24*) revealed another striking difference with possible functional implications. When superimposing the two structures, we observed that, in the human receptor, AM580 inserts its tetramethyl-cyclohexyl ring between helices H3 and H11, whereas in the annelid RAR, the β-ionone ring of ATRA resided deeper within the LBP (Fig. 3F). As a consequence, helices H3 and H11 are closer to each other in the liganded PduRAR, hence generating a possibly suboptimal docking surface for helix H12 in the transcriptionally active conformation (Fig. 3, F and G). Moreover, although direct contacts exist between agonist ligands and helix H12 residues (I410 and L414) in human RARα, no such interactions were observed in the ATRA-bound PduRAR (Fig. 3F). These observed structural differences between the annelid and human RAR LBDs suggested that ATRA only weakly stabilizes the active conformation of helix H12 in the PduRAR. This finding explained both the dissociation of helix H12 from its LBD core in the B and D subunit structures and the significantly weaker ATRA-induced transcriptional activity of the annelid receptor in cell-based assays, when compared to the activity of a typical human RAR (fig. S4D).

Together, our functional and structural data indicate that PduRAR is able to bind different RA isomers (at least ATRA, 13cRA, and 9cRA) with a micromolar affinity by using distinctive ligand-binding modes and structural responses when compared to vertebrate RARs. Thus, PduRAR likely behaves as a sensor rather than as a high-affinity receptor.

Retinoids in developing and adult *P. dumerilii*

To test whether RA is present in *P. dumerilii*, we next determined the retinoid contents in eggs, embryos, larvae, and adults using liquid chromatography–tandem mass spectrometry (LC-MS/MS) for RA (*4*, *25*) and high-performance liquid chromatography with ultraviolet detection (HPLC-UV) for retinol and retinyl esters (*4*). We were able to identify ATRA, 13cRA, retinol, and retinyl esters but failed to detect 9cRA above the limit of detection of our assay (Table 1) (*25*). The concentrations of ATRA and 13cRA were in the same range, and often, 13cRA was present at higher levels than ATRA (Table 1). For example, in *P. dumerilii* adults, we detected 38.3 ± 4.03 pmol/g tissue of ATRA and 46.8 ± 3.89 pmol/g tissue of 13cRA (Table 1), with one unit of pmol/g tissue of a given retinoid translating, approximately, into an average concentration of 1 nM (*26*). This finding contrasts with the situation in vertebrates, where ATRA levels generally tend to be higher than those of 13cRA (*26*).

Retinoids were further quantified in unfertilized eggs and at different developmental stages: 18 hours post-fertilization (hpf) (gastrulating protrochophore), 51 hpf (early metatrochophore larva), and 74 hpf (early nectochaete larva) (*17*). The relative levels of ATRA and 13cRA were generally lower during embryogenesis than in the adult, in accordance with the notion that embryonic retinoids are synthesized from precursor molecules stored in the egg, whereas, in adults, precursors are obtained from the diet. During embryogenesis, ATRA levels were highest during gastrulation (4.58 ± 0.16 pmol/g tissue), whereas 13cRA levels were highest in 51 hpf larvae (7.47 ± 4.63 pmol/g tissue) and gastrulating embryos (6.34 ± 2.21 pmol/g tissue) (Table 1). These results suggest that, as in vertebrates, active retinoid levels are tightly controlled, although the kinetics of ATRA and 13cRA levels during *P. dumerilii* embryogenesis differ, suggesting distinct control mechanisms. Furthermore, given that ATRA and 13cRA levels were assessed in whole animals, we expect that RA concentrations are significantly higher in target tissues, hence leading to the ligand-dependent activation of PduRAR.

Retinol and retinyl esters serve as precursors for the synthesis of RA in vertebrates (*3*, *27*). In *P. dumerilii*, we observed much higher levels of retinol and retinyl esters than of ATRA or 13cRA (Table 1), similar to what is observed in vertebrates (*3*, *4*, *26*), which suggests that these retinoids also serve as precursors for RA synthesis in the annelid. The

Table 1. Endogenous retinoids in *P. dumerilii*. Values are means ± SD. Serum values are pmol/g tissue. n.d., not detected. Developmental stages correspond to gastrulation at 18 hpf, the early metatrochophore larva at 51 hpf, and the early nectochaete larva at 74 hpf.

Stage	ATRA	9cRA	13cRA	Retinol	Retinyl esters
Unfertilized egg (n = 4)	0.92 ± 0.74	n.d.	0.73 ± 0.41	50 ± 31.25	180 ± 68.66
Gastrulating protrochophore (n = 2)	4.58 ± 0.16	n.d.	6.34 ± 2.21	420 ± 200	1000 ± 417.81
Early metatrochophore larva (n = 9)	2.74 ± 1.52	n.d.	7.47 ± 4.63	830 ± 489.34	1880 ± 1004.92
Early nectochaete larva (n = 6)	3.39 ± 1.10	n.d.	2.53 ± 1.17	300 ± 125.65	900 ± 567.46
Adult worm (n = 4)	38.3 ± 4.03	n.d.	46.8 ± 3.89	878.5 ± 102.3	22170 ± 4581

fact that retinol and retinyl ester levels are higher in gastrulating embryos than in eggs suggests that retinoids are stored in other forms in the oocyte and that, when embryonic transcription starts, retinol and retinyl esters are synthesized from these alternatively stored retinoids.

Expression of genes involved in RA synthesis, signaling, and degradation

The biosynthesis of RA is best tracked by studying genes involved in its metabolism. In vertebrates, RALDH enzymes are enriched in somatic tissues at the interface between the yolk sac and the embryo (*28*). In *P. dumerilii*, three of five *aldh1a* paralogs (*aldh1a_1*, *aldh1a_4*, and *aldh1a_5*), which are likely involved in RA synthesis, were found in the yolky macromeres (fig. S5, A, B, C, E, F, H, and J to M) and in the adjacent mesodermal bands that stretch out between the macromeres and the overlying neuroectoderm (fig. S5, F and G). This expression is in line with the notion that RA metabolism takes place in the annelid yolk and that oxidation to RA is performed either in the yolk itself or in the overlying early-forming somites. Once the midgut is formed, the three *aldh1a* genes were expressed in tissues surrounding the midgut, suggesting a function related to food intake and the control of metabolism (fig. S5, D, I, and N). A fourth *aldh1a* gene, *aldh1a_3*, was expressed in other tissues (fig. S5, O to R). The in situ hybridization experiments targeting the fifth *P. dumerilii aldh1a* paralog, *aldh1a_2*, did not yield any results, which is likely due to low developmental expression levels. The three *P. dumerilii cyp26* genes (*cyp26_1*, *cyp26_2*, and *cyp26_3*) showed expression in the midgut, which is consistent with a possible modulation of RA activity in this tissue (fig. S5, S to U).

To determine where the RA signal is received, we analyzed the expression of the annelid RAR and RXR. The first prominent expression of the *rar* gene was in the larval neuroectoderm (Fig. 4, A to C), and at 48 hpf it was spatially restricted to the medial domain (Fig. 4C), where *pax6* and *nk6* expression overlap and *hb9*+ motor neurons differentiate (*29*). Lateral neuroectoderm was devoid of expression. At the same time, *rar* was also expressed in the brain (Fig. 4, A to D) and in the developing mesodermal bands in the trunk (Fig. 4, A to C). Starting between 24 and 30 hpf, the *rar* gene was further detectable in the developing stomodeum and proctodeum, where it remained expressed until 72 hpf (Fig. 4, B to D). Furthermore, in the young worm, *rar* was expressed in the midgut (Fig. 4E). Coherent with a possible dimerization of RAR and RXR, the *rxr* gene was expressed at similar stages in the same tissues (neuroectoderm, brain, mesoderm, stomodeum, and midgut) (Fig. 4, F to I). Together, the expression patterns of the main RA signaling components in *P. dumerilii* (Fig. 4, J to M) are consistent with the notion that endogenously produced RA activates RAR/RXR heterodimers in a tissue-specific manner to function during development of the nervous system and the alimentary canal.

Medial neuron differentiation and connective formation defects in RAR and RXR knockdowns

The overlapping neuroectodermal expression of *rar* and *rxr* genes in conjunction with the ability of both receptors to form heterodimers suggests a functional interaction in vivo to control nervous system development. To test this hypothesis, we targeted *rar* and *rxr* translation by a morpholino oligonucleotide (MO) knockdown approach. As a first test for the capacity and specificity of the synthesized MOs to inhibit translation in *P. dumerilii*, we injected, into one-cell– to two-cell–stage embryos, *h2b-gfp* mRNA with an upstream MO target sequence together with the *rar* MO, *rxr* MO, or 5-mismatch control MOs. We found that both the *rar* and *rxr* MOs specifically abolished green fluorescent protein (GFP) expression of their respective mRNAs (fig. S6) and noted a general developmental delay for all MO injections (Fig. 5), which is consistent with previous reports on the use of MOs in developmental systems (*30*).

Larvae injected with *rar* MO developed regularly into larval stages (98%, $n = 363$), comparable to controls (98%, $n = 196$). To score for morphological effects, we labeled fixed larvae with 4′,6-diamidino-2-phenylindole (DAPI) and with an antibody directed against acetylated tubulin that labels axons and cilia (*29*, *31*). Morphological defects became apparent in the fully developed metatrochophore larva, with aberrant axonal scaffolds in the differentiating ventral nerve cord that were clearly distinct from control MO-injected scaffolds (Fig. 5, A, C, E, and I). The *rar* morphants exhibited overall reduced connectives (50%, $n = 22$), whereas commissural axons appeared less affected (Fig. 5, C and E). Although commissural trajectories were partially disorganized, the capacity of axons to cross the midline was not impaired (Fig. 5, C and E). We also analyzed larvae injected with *rxr* MO and found them to be overall morphologically very similar to the *rar* MO–injected ones, characterized by a specific reduction of connectives and altered commissural bundling (75%, $n = 60$) (Fig. 5, G and I). In addition, we observed a behavioral effect in *rxr* MO–injected larvae in that some did not swim but rather stayed on the bottom of the dish, although they were agile and appeared normally developed (55%, $n = 286$).

Analysis of *synaptotagmin* expression, a marker for presynaptic differentiation, in *rar* morphants revealed a specific decrease of neurons in the medial trunk domain that differentiates between 22 and 56 hpf (*29*), whereas earlier forming larval neurons were unaffected (100%, $n = 4$) (Fig. 5, L and M). This suggests a specific requirement for RA signaling in larval neuronal differentiation in the medial neuroectoderm. To corroborate this point, because serotonin is an abundant neurotransmitter in both the larval nervous system and the ventral nerve cord (*29*), we investigated the development of serotonergic neurons in *P. dumerilii rar* and *rxr* morphants. We found that, after both *rar* and *rxr* MO injections, the early developing, embryonic serotonergic neurons were unaffected, whereas the number of the later differentiating, larval serotonergic neurons was reduced (Fig. 5, B, D, F, H, J, and K). This reduction was more pronounced in terminally differentiated serotonergic neurons (with axons) (Fig. 5K) than in differentiating serotonin-positive cells (without axons) (Fig. 5J).

We next assessed the expression of the transcription factor *hb9*, which specifically marks motor neurons differentiating from the medial neuroectoderm in both annelids (*29*) and vertebrates (*32*). In *P. dumerilii* larvae injected with *rar* MO, we found reduced *hb9*-expressing cells (55%, $n = 9$) (Fig. 5, N and O). Finally, we tested whether the failure to differentiate medial nerve cord neurons is due to disturbed larval patterning mediated by *hox* genes, which, in *P. dumerilii*, show spatial colinear expression along the trunk neuroectoderm (*33*). Contradicting this notion, the segmental expression of *hox1* in the neuroectoderm was not affected by *rar* MO injections (100%, $n = 20$) (Fig. 5, P and Q).

In line with *rar* and *rxr* expression in the stomodeum, which later develops into the larval foregut, we further observed a duplication (18%, $n = 22$) or enlargement (27%, $n = 22$) of the stomodeum after *rar* MO injections (Fig. 5, A, C, E, and I), indicating that the reception of an endogenous RA signal is also required for proper stomodeal development. Comparable stomodeum duplications (8%, $n = 60$) or enlargements (16%, $n = 60$) were also observed in *rxr* knockdown specimens (Fig. 5, G and I).

Finally, coinjection of the *rar* and *rxr* MOs (at lower concentrations) resulted in phenotypes identical to those obtained by single MO

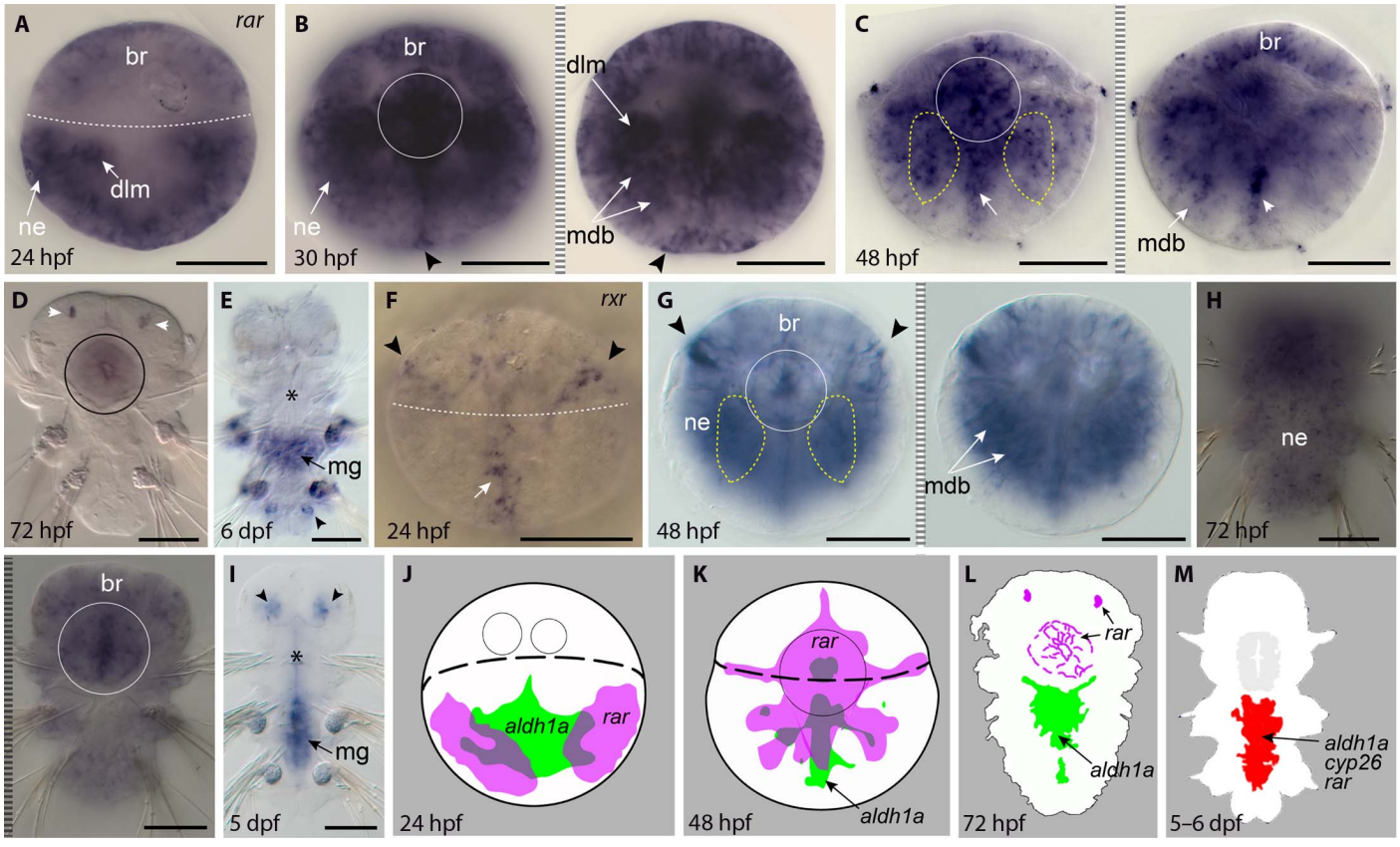

Fig. 4. Expression of retinoid receptors (*rar* and *rxr*) in *P. dumerilii*. Gene expression is shown in blue. (**A** to **E**) *P. dumerilii rar* expression. (A to C) *rar* expression in forming neuroectoderm (ne), mesodermal precursor cells [dorsal longitudinal muscle (dlm) and mesodermal bands (mdb)], posterior growth zone (black arrowheads), and the brain region (br). (C) At 48 hpf, *rar* is expressed in neuroectoderm, in a region giving rise to motor neurons (yellow dashed circles), in the ventral midline (arrow, left) and subjacent cells (white arrowhead, right). (B to D) Stomodeal *rar* expression at 30 to 72 hpf (circles). (D) *rar* is expressed in two dorsally located domains of the brain at 72 hpf (white arrowheads). (E) At 6 dpf (days post-fertilization), *rar* is expressed in the midgut (mg) and posterior growth zone (black arrowhead). (**F** to **I**) *P. dumerilii rxr* expression. (F) At 24 hpf, *rxr* is expressed in the ventral midline (arrow) and two domains of the brain (black arrowheads). (G and H) In trochophore and nectochaete larvae, *rxr* is expressed in the brain (br) and the entire neuroectoderm (ne), including motor neuron domains (yellow dashed outline), and in the underlying mesodermal precursor cells (mdb) and stomodeum (circle). (I) By 5 dpf, *rxr* expression is restricted to two domains of the brain (arrowheads) and to tissues surrounding the midgut (mg). (**J** to **M**) Summary of the developmental expression in *P. dumerilii* of RA metabolism and signaling components. At 24 hpf (J), 48 hpf (K), and 72 hpf (L), *aldh1a* (green) genes are expressed in the blastoporal region and macromeres, whereas *rar* (purple) is in neuroectoderm and stomodeum. *aldh1a* and *rar* expression overlap in the forming mesodermal bands. (M) In the late nectochaete larva (5 to 6 dpf), *aldh1a*, *cyp26*, and *rar* expression overlap in the midgut (red). Ventral views of larvae are shown. Scale bars, 50 μm. * or circle, foregut; white dashed line, ciliated band; yellow dashed circles, motor neuron domain.

injections in both ventral nerve cord and stomodeum (Fig. 5I), indicating that RAR and RXR cooperatively function in the same signaling cascade as RAR/RXR heterodimers mediating RA signaling during *P. dumerilii* development.

Enhanced commissural axon formation induced by ectopic RAR activity

To complement the MO-based knockdown results, we injected mRNAs encoding the full-length RAR protein into *P. dumerilii* zygotes. Ectopic expression of *rar* led to alterations of axonal scaffolds at the end of the larval differentiation phase (Fig. 5, T to V), in line with the phenotypes of *rar* MO–injected larvae. In *rar* mRNA–injected larvae fixed at 48 hpf, we observed an increase in the formation of commissural axons, whereas the formation of longitudinal connectives appeared unaffected (Fig. 5, T and U). The ectopic commissural axons most likely emerge from the more lateral neuroectodermal regions (*29*), where commissural neurons are located in wild-type larvae. Notably, *rar* mRNA–injected larvae fixed at early larval stages (at 41 hpf) did not show a phenotype in the ventral nerve cord, which is consistent with the notion that, during neurogenesis, endogenous RAR-dependent signaling is required at larval rather than prelarval stages (Fig. 5, R, S, and V). Together, the results of the *rar* overexpression and knockdown experiments are consistent with a role for RAR in neuronal differentiation and axon formation within the medial part of the larval *P. dumerilii* neuroectoderm.

Impaired medial neuron differentiation by neuroblast depletion following ATRA and 13cRA treatments

To further investigate the roles of RA signaling in larval ventral nerve cord development, we assessed the effects of exogenous ATRA and 13cRA, the two active RA isomers present during *P. dumerilii* development. Larvae were treated with increasing concentrations of both compounds in the micromolar range. Both ATRA and 13cRA treatments at larval stages slowed down the locomotion of the larvae and completely abolished crawling movements (movie S1), which is indicative of a specific effect on the differentiation and possibly projection of motor neurons innervating the somatic musculature. For comparison,

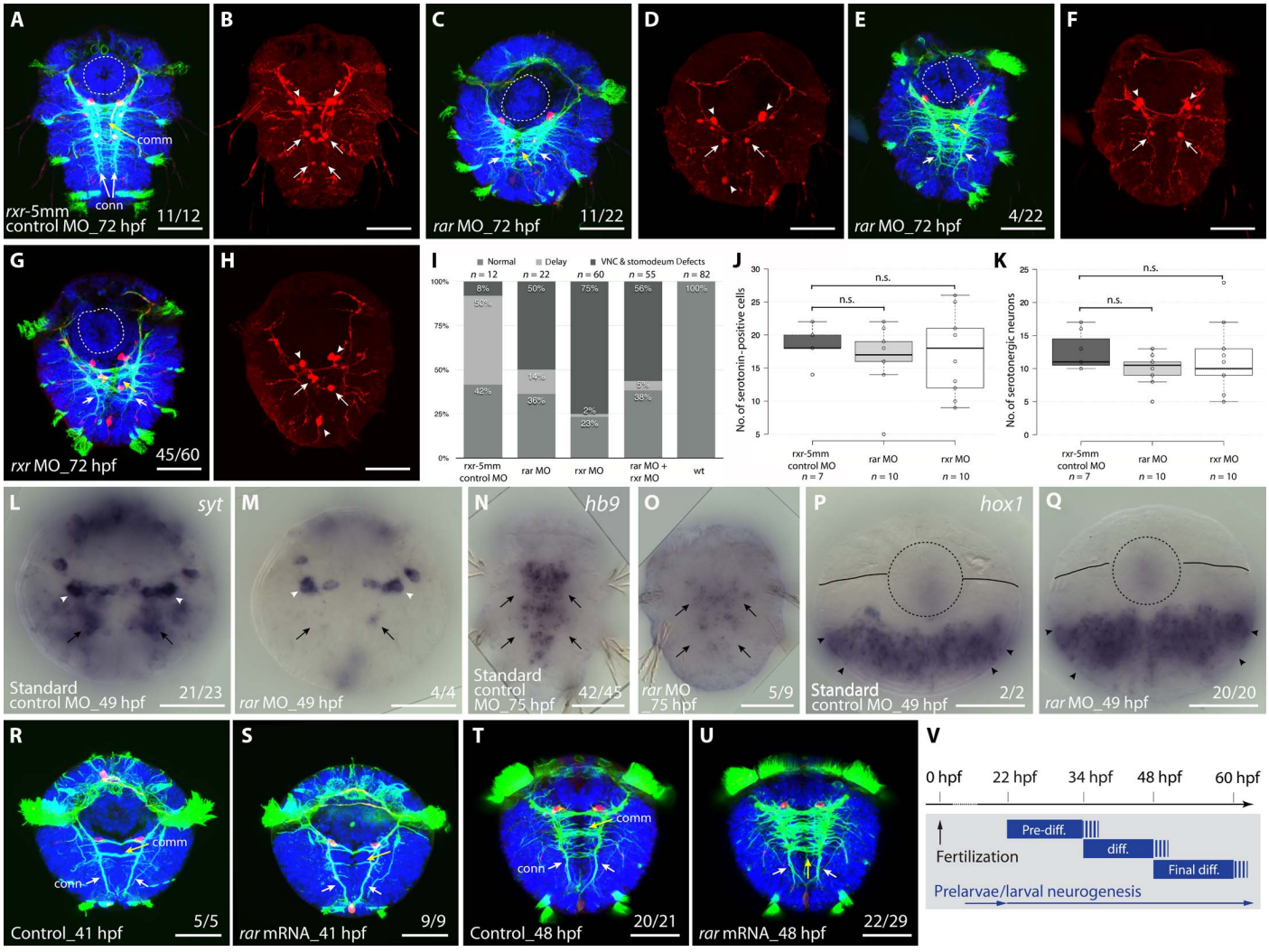

Fig. 5. Perturbation of RAR and RXR functions in *P. dumerilii*. (**A** to **Q**) Knockdown of *rar* and *rxr* by MO injections into *P. dumerilii* zygotes. (A, C, E, and G) *rar* and *rxr* MO injections cause a reduction of connectives (conn; white arrows) and misguidance of commissures (comm; yellow arrows) in the ventral nerve cord (VNC) as well as stomodeal defects including duplications (white dashed circle). (B, D, F, and H) Misplacement and reduction of larval serotonergic neurons (arrows), but not of neurons of the early nervous system (arrowheads), upon *rar* and *rxr* MO injections. (I) Histogram showing proportions of obtained knockdown phenotypes: normal development ("normal"), delayed development ("delay"), and VNC and stomodeum defects ("VNC & stomodeum defects"). (J and K) Box plots showing the number of serotonergic cells and neurons in the trunk of *P. dumerilii* larvae. Data distribution (circles), median values (bold line), and Tukey whiskers are shown. wt, wild type. Unpaired *t* test on the mean value was used for statistical analyses (n.s., nonsignificant). $P = 0.3352$ and $P = 0.5842$ in (J) and $P = 0.0566$ and $P = 0.6064$ in (K) for, respectively, *rxr*-5mm control MO versus *rar* MO and *rxr*-5mm control MO versus *rxr* MO. (L to O) Expression of the neuronal differentiation marker *synaptotagmin* (*syt*) (L and M) and of the motor neuron marker *hb9* (N and O), showing that MO-induced *rar* knockdown disrupts differentiation in the larval nervous system (arrows), but not in the early larval nervous system (arrowheads). (P and Q) *hox1* expression is unaffected by *rar* MO injections (arrowheads). (**R** to **U**) *rar* overexpression by mRNA injection into *P. dumerilii* zygotes. (R and S) Early larval nervous system is not affected by *rar* overexpression (arrows). (T and U) Injection of *rar* mRNA induces an increase of commissures in the larval nervous system (arrows). (**V**) Overview of embryonic and larval neurogenesis in *P. dumerilii* with respect to the differentiation (diff.) of functional neurons (*29*). Ventral views of larvae are shown. (A to H and R to U) Acetylated tubulin in green, serotonin in red, and nuclei in blue. (L to Q) Gene expression in blue. Number of affected over total number of assayed specimens is indicated. Scale bars, 50 μm.

similar treatments did not slow down the swimming speed of prelarvae (movie S2).

Concerning axonal scaffold formation, treatments with both compounds from 48 to 80 hpf led to a clear concentration-dependent reduction in length and density of longitudinal connectives, with the overall number of commissural projections being less affected (Fig. 6, A to E and P). Of note, 13cRA treatments resulted in more severe phenotypes than ATRA treatments at the same concentration. Corroborating this further, treated larvae generally showed a reduction of differentiated serotonergic neurons that are longitudinally projecting, an effect, again, more pronounced for 13cRA than for ATRA treatments (Fig. 6, F to J and Q). ATRA and 13cRA further decreased the number of *hb9*-positive cells in the neuroectoderm but not in the stomodeum (fig. S7, A to F). In contrast, the anterior spatial boundary of the neuroectodermal expression of *hox1* and *hox4* was unaffected (fig. S7, G to I and M to O), whereas that of *hox1* at the base of the cirri and in the stomodeum was downregulated (fig. S7, J to L). Therefore, and strikingly, *rar* MO–injected and RA-treated larvae showed very similar phenotypes.

Counterintuitive at first, we reasoned that if RA acted as a motor neuron differentiation signal, it might interfere with the maintenance of asymmetrically dividing neuroblast stem cells in the neuroectoderm. Consistent with this notion, we noted a marked reduction of cell division in the neuroectodermal tissue in both ATRA- and 13cRA-treated larvae after 4 hours of 5-ethynyl-2′-deoxyuridine (EdU) incubation, whereas cell proliferation in the brain appeared largely unaffected (Fig. 6, K to O). To more specifically test for the presence of neuroblasts in treated young worms, we assessed neuroectodermal *nk6* and *pax6* expression at early larval stages, which demarcates both proliferating stem cell–like neuroectodermal precursors and differentiating neurons (*29*). In line with the above observations, the expression of both markers was strongly reduced in a concentration-dependent manner after treatments at early larval stages (Fig. 6, R to T and V to X). Optical cross-sections revealed that the expression of both genes was reduced in deep tissue layers, where differentiating neurons are located and completely abolished in superficial layers containing dividing neuroblasts (Fig. 6, U and Y). Therefore, the reduced number of differentiating motor neurons appears to be paralleled by a depletion of neuroblasts giving rise to these neurons, which suggests that the effect of RA treatment is on the dividing stem cells rather than their differentiating descendants.

DISCUSSION

We have exhaustively characterized RA signaling, both biochemically and functionally, in the developing marine annelid *P. dumerilii*. Our work establishes firmly that RAR-mediated RA signaling evolved in early bilaterians. However, our data also suggest an early role of this pathway very different from the control of *hox* anteroposterior patterning that has been described for vertebrates.

First, the affinity of the PduRAR for its ligands (ATRA or 13cRA) and its level of activation by these ligands are much lower than those known for vertebrate receptors. For the annelid receptor, micromolar retinoid doses were necessary to reach $^{1}/_{10}$ of the transcriptional activity measured for human RARα at nanomolar retinoid concentrations (*8*). Our structural analyses established that PduRAR accommodates ATRA via a binding mode that is different from the one used by vertebrate RARs. In the *P. dumerilii* orientation, the ligand does not generate the necessary contacts with residues of the RAR LBP to ensure high-affinity binding and strong stabilization of the transcriptionally active receptor conformation. Given that endogenous retinoid levels do not seem to be overtly elevated in both developing and adult worms, when compared to those in vertebrates (*3*, *4*, *26*), the annelid RAR thus appears to act as a retinoid sensor rather than as a vertebrate-type high-affinity receptor. Such a sensor role is exerted in tissues that are characterized by high exposure to RA, such as the neuroectoderm overlying the RA producing mesodermal bands and midgut. It is further supported by the fact that PduRAR is activated by ATRA and 13cRA, which are present in equivalent amounts in embryos and adults. In line with our data, the RAR of the sea urchin, a deuterostome, is characterized by a ligand affinity comparable to that of PduRAR (*34*). Together, these results indicate that the ancestral RAR, which evolved at the base of the bilaterians, might have been a retinoid sensor and that high-affinity RARs probably evolved only later, specifically in the chordate lineage.

Second, the affinity refinement of chordate RARs was very likely correlated with other modifications of the RA pathway. For example, our study revealed that annelids differ from chordates in the complements of retinoid binding and transport proteins (that is, STRA6, RBP4, TTR, CRBP, and CRABP), all of which are absent from annelids. This suggests that the ancient mode of signal propagation was by mere diffusion (both extra- and intracellularly) or that retinoid binding and transport have primitively been assumed by other factors and that this primitive system has secondarily been replaced in chordates. An intracellular retinoid binding capacity, for example, has already been described for members of the ILBP (intracellular lipid binding protein) superfamily in other protostomes, such as insects and crustaceans (*35*, *36*).

Third, another pivotal difference between the annelid and chordate RA systems is the absence of an axial patterning function in annelids, together with the lack of a direct regulation of *hox* genes. This classical and well-known developmental function of RA signaling has so far only been demonstrated in chordates, although it still remains to be addressed in echinoderms and hemichordates. Therefore, this role of RA can be considered either a deuterostome or chordate synapomorphy, and it may have evolved concomitantly with the elaboration of high-affinity RARs. The echeloned response of different *hox* genes to RA would thus be the consequence of a gain of regulatory precision by a high-affinity receptor that is capable of interpreting minute ligand concentration differences along an anteroposterior morphogen gradient. In chordates, this gradient provides positional information along the anteroposterior body axis to specify the location and fates of particular structures in all germ layers (*2*). In zebrafish, for example, it has been shown that RA can directly convey tiered positional information over long distances, functioning in a gradient that is robust to fluctuations of RA synthesis and whose establishment requires CYP26-dependent RA degradation (*37*). Together, we propose that the transformation of RAR from a sensor to a high-affinity receptor, which likely took place at the base of the chordates, was a prerequisite for the acquisition of a global axial patterning function of RA as a gradient-forming morphogen.

On the basis of these findings and additional comparative studies, a coherent view of RA signaling evolution is emerging. Early in metazoan evolution, retinoids appear to have been recruited as signaling molecules. Although RAR itself is absent in cnidarians, the existence of RXR orthologs activated by 9cRA indicates the existence of nuclear receptors capable of mediating retinoid actions (*38*), possibly as homodimers or heterodimers with other nuclear receptors (*39*). In cnidarians, two major roles have emerged that may be derived from ancient RA signaling functions. First, RA controls the strobilation process in the jellyfish *Aurelia aurita*, that is, the metamorphosis from the polyp to the medusa stage (*39*). During this process, RA appears to be produced by the inner layer because the expression of *raldh* is strongest in the endoderm of the mouth region, where strobilation is initiated. In contrast, *rxr* is present in the overlying ectoderm. Second, RA signaling appears to play an ancient role in neuronal differentiation. An RXR antibody labels different types of neurons in the polyps of the sea pansy *Renilla koellikeri* and the coral *Acropora millepora* (*40*), suggesting a role in neurogenesis. In line with this hypothesis, RA induces neuronal differentiation in *R. koellikeri* primary cell cultures (*41*), and RA-treated planula larvae of the hydrozoan *Clava multicornis* showed defects in the differentiation and positioning of peptidergic neurons and, interestingly, a disorganized arrangement of nerve net axons, indicative of an RA function in axonal pathfinding (*42*).

Two major novelties in RA signaling then occurred in the bilaterian stem line. First, RXR was complemented by a second RAR, which forms heterodimers with RXR (*8*). We propose that, via opportunistic evolution, RAR evolved as an RA sensor by exploiting preexisting retinoids. This involved changes in specificity, from 9cRA (as reported

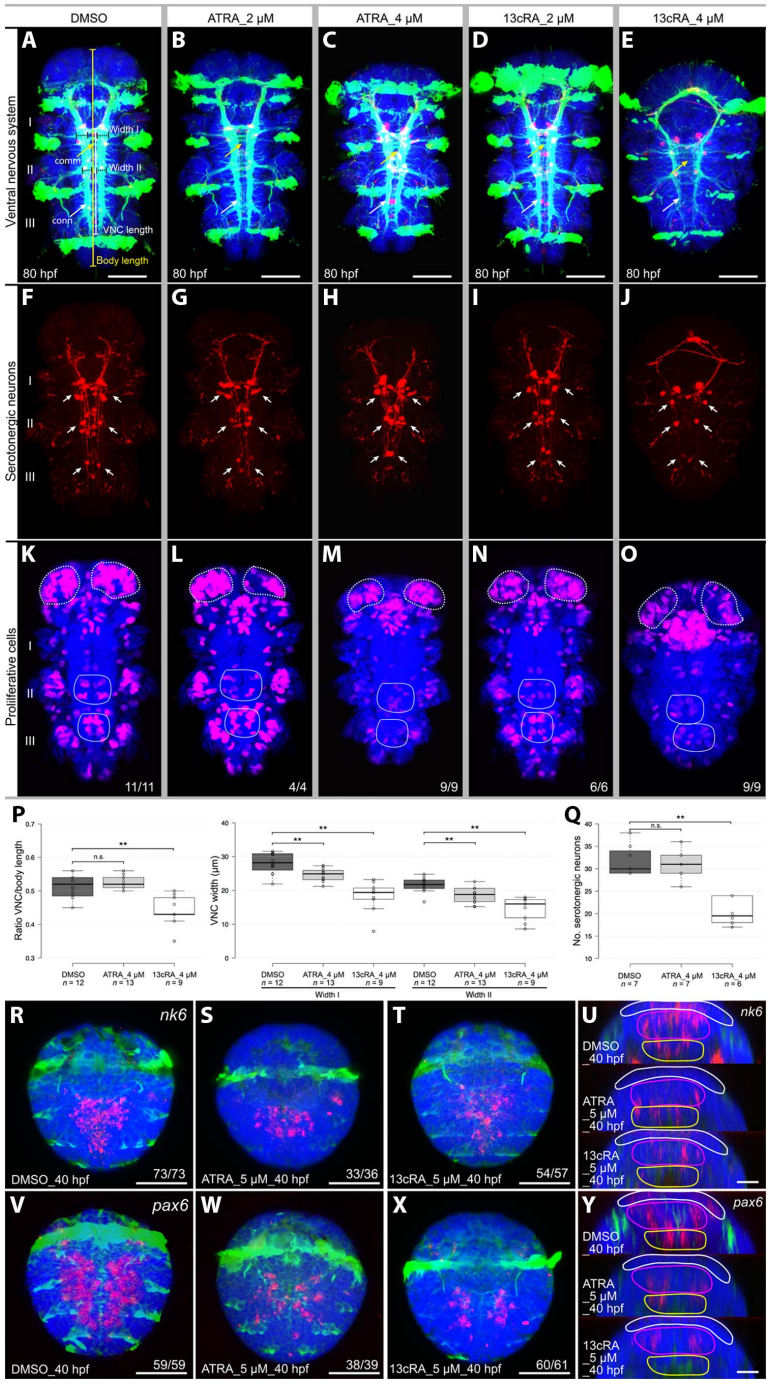

Fig. 6. Effects of exogenous RA on developing *P. dumerilii*. (**A** to **Q**) Effects of ATRA and 13cRA on larval development (48 to 80 hpf). (A to E) Reduction of differentiation within the VNC (in green, acetylated tubulin), particularly in longitudinal connectives (conn; white arrows) and less in commissural projections (comm; yellow arrows), was observed with increasing RA concentrations. (F to J) Treatments reduce the number of differentiating serotonergic neurons (in red, serotonin) along the VNC (arrows). (K to O) Number of proliferating cells (in purple, 4-hour EdU incubation) in larval neuroectoderm (circles) is reduced by ATRA and 13cRA, whereas cell proliferation in the larval brain is less affected (dashed circles). (A, F, and K) The first (I), second (II), and third (III) larval segments are indicated. (P and Q) Box plots of VNC length and width and of serotonergic neuron numbers in dimethyl sulfoxide (DMSO) controls and after treatments with 4 µM ATRA or 4 µM 13cRA. Data distribution (circles), median values (bold line), and Tukey whiskers are shown. Unpaired *t* test on the mean value was used for statistical analyses (**$P < 0.01$). (P) Ratio of VNC length and total body length, as shown in (A), and comparison of VNC width in the first two body segments, indicated as width I and II in (A). Left box plot: $P = 0.4048$ for DMSO versus ATRA and $P = 0.0006$ for DMSO versus 13cRA. Right box plot: $P = 0.002$ and $P = 0.0001$ (width I) and $P = 0.0017$ and $P = 0.0001$ (width II) for, respectively, DMSO versus ATRA and DMSO versus 13cRA. (Q) Serotonergic neuron numbers in DMSO-, ATRA-, and 13cRA-treated embryos. $P = 0.6504$ for DMSO versus ATRA and $P = 0.0001$ for DMSO versus 13cRA. (**R** to **Y**) Treatments reduce *nk6* (R to T) and *pax6* (V to X) expression in the VNC during larval development (34 to 40 hpf). Gene expression in pink. (U and Y) Orthogonal optical sections showing the absence of *nk6* and *pax6* from proliferating neuroectoderm (superficial layer, white outline) and decrease of *nk6* and *pax6* expression in the postmitotic layers below the neuroectoderm (middle and deep layers, purple and yellow outlines, respectively). Ventral views of developing *P. dumerilii* are shown. Number of affected over total number of assayed specimens is indicated. Scale bars, 50 µm [except (U) and (Y), 20 µm].

for cnidarians) to 13cRA and ATRA (as prevalent in bilaterians), which thus likely enabled and triggered a diversification of the downstream effectors of RA signaling. Second, and concomitant with RAR, another key actor of the pathway (namely CYP26) evolved, mediating RA degradation. Targeted RA catabolism evolved to allow spatially and temporally refined RA signaling activity by removing the active ligand from exempt tissue. We therefore propose that the origin of RAR and CYP26 in bilaterians coincided with the appearance of specific biological roles for RA and with the need for a precise spatiotemporal control of RA availability.

But what was the effect of such refined signaling? Application of ATRA to individual neurons isolated from the central nervous system of the gastropod mollusk *Lymnaea stagnalis* causes neurite outgrowth and growth cone turning (*43*), as it does in the vertebrate spinal cord, for example, in the chick embryo (*44*) and the regenerating adult newt (*45*), supporting the notion that axonal guidance is an ancient function. Unfortunately, these studies in gastropod mollusks left open the source of the signal and the nature of the receptor and did not address a possible role in neuronal patterning or differentiation. Our study now reveals that, during *P. dumerilii* development, RA produced by the underlying mesodermal bands and midgut triggers neuronal differentiation in the overlying neuroectoderm. More specifically, we observe effects on differentiating motor neurons in the trunk of three-segmented young worms, coupled with disorganized patterns of outgrowing axons. These results are consistent with a role of RA signaling in axonal pathfinding of motor neurons and associated interneurons, and, in more general terms, with the somatic musculature promoting its own innervation from motor neurons at various steps (neuroblast proliferation, differentiation, and axonal outgrowth). A similar role in neuronal differentiation has been reported for vertebrates (*46*), which is independent of the famous early role of RA signaling in *hox*-mediated anteroposterior patterning. For example, in zebrafish *neckless* mutants with a defect in *raldh2*, the differentiation of branchiomotor neurons is disturbed, involving also migration defects and a disorganized axonal scaffold (*28*, *47*). Transplantation experiments have shown that the RA signal originates in the underlying developing somatic musculature, as observed here for the annelid. This opens up the fascinating possibility that the evolution of RAR has been linked initially to the evolution of bilaterian motor circuits, enabling the usage of retinoids as a developmental timing signal at multiple steps of specification and differentiation.

Such an initial role in the control of differentiation of motor and interneurons may elegantly explain the recruitment of RA signaling for anteroposterior patterning via *hox* gene regulation. One pivotal role of the *hox* network is to specify the different types of motor neurons

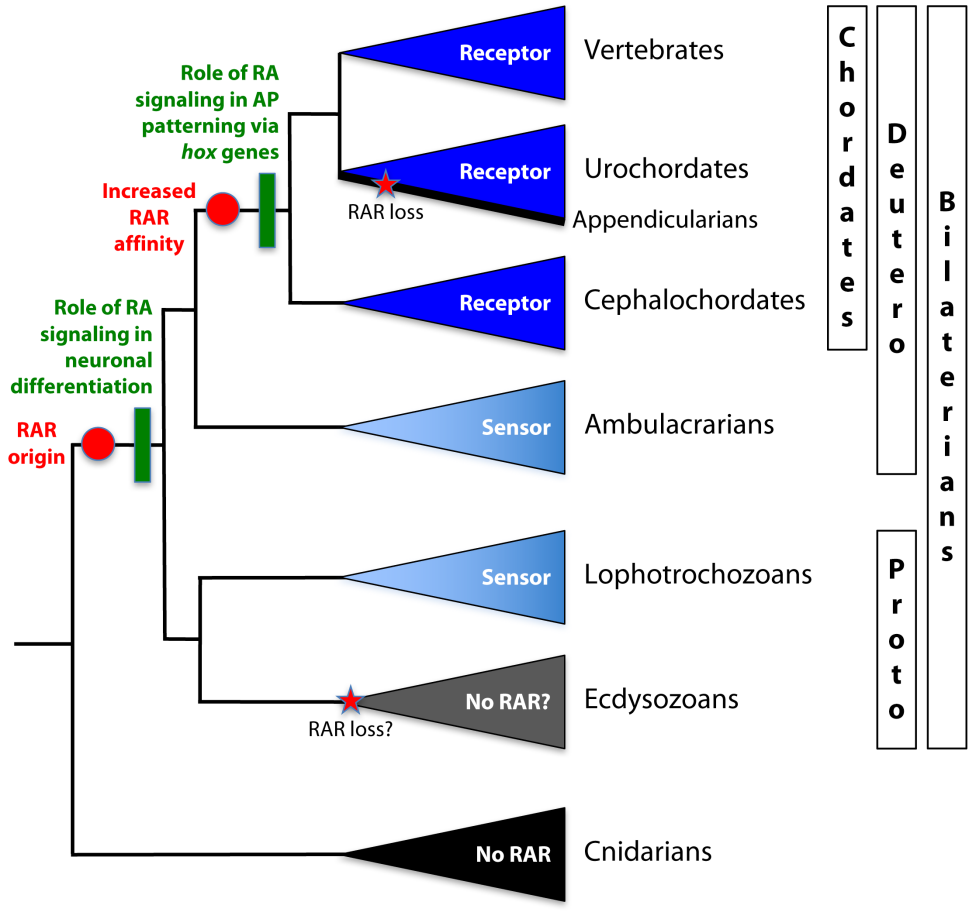

Fig. 7. A simplified phylogeny of metazoan animals illustrating major events of RA signaling evolution. The color used for each taxon highlights the RA binding capacity of the RAR: light blue for low-affinity sensors and dark blue for high-affinity receptors. Red circles highlight hypothesized events of RAR evolution, and green boxes highlight the likely concomitant appearance of the two main developmental roles of RA signaling: in neuronal differentiation at the base of bilaterians and in anteroposterior (AP) regional patterning via *hox* gene regulation at the base of chordates. Red stars indicate secondary RAR loss. Deutero, deuterostomes; Proto, protostomes.

innervating the fore- and hindlimbs along the anteroposterior axis—and this is a direct readout of high-affinity RA signaling (*48*). It is thus conceivable that the role of RA signaling in *hox* regulation evolved as a result of "opportunistic evolution": Because RA signaling control of general motor neuron differentiation was already in place, RA was also recruited as a signal for the more specific spatial control of anteroposterior subtype specification that evolved progressively in fins and limbs, and, in this context, took over the (refined) control of anteroposterior *hox* gene expression. This way, and reflecting its overall and more ancient role in the coordination of developmental timing, RA signaling would then have become a global regulator of *hox* gene expression in deuterostomes—likely at the base of chordates—to control the elaboration of the anteroposterior body axis (Fig. 7).

MATERIALS AND METHODS

Experimental design

The objectives of the presented research were to understand the ancestral role of the RA signaling pathway, mediated by RAR. Using the annelid worm *P. dumerilii* as model organism, we approached our biological question by means of a combination of different in silico, in vitro, and in vivo approaches to identify RA signaling pathway components, assess the molecular properties and crystal structure of RAR, establish in vivo retinoid contents, define the developmental expression of the main RA signaling mediators, and characterize the functions of both RA and RAR during development. The functional experiments were analyzed by behavioral studies (recording of the swimming behavior of the larvae) and by immunohistochemistry (protein localization) and in situ hybridization (gene expression patterns) on fixed control and experimental specimens of *P. dumerilii* embryos or larvae. The investigators carrying out these analyses were blinded to the identities of the samples (that is, control versus experimental). Retention of microinjected embryos in the analysis was based on the pattern of early development (correct initial cell divisions and fusion of the small lipid droplets into four bigger lipid droplets). Deviation from this early developmental pattern is a sign of traumatization and thus of damage to the embryo caused by the microinjection procedure (*17*). Biological and technical replicas are indicated for each experiment.

Sequence alignments and phylogenetic analyses

Sequences for in silico analyses of retinoid metabolism and signaling components were retrieved by reciprocal Basic Local Alignment Search Tool (BLAST) searches from the databases implemented at the National Center for Biotechnology Information. Species included were the cnidarian *Nematostella vectensis*, the mollusk *Lottia gigantea*, the annelid *C. teleta*, the amphioxus *Branchiostoma floridae*, the fish *Danio rerio*, and humans, that is, *Homo sapiens*. Possible orthologs from *P. dumerilii* were retrieved from transcriptome databases of the Arendt (http://4dx.embl.de/platy/) and Jékely (*49*) laboratories by reciprocal BLAST searches. Sequence alignments were initially computed using MUSCLE (*50*) and subsequently refined manually. Phylogenetic analyses were calculated with both the maximum likelihood (ML) and Bayesian inference (BI) methods. The ML trees were constructed with PhyML v3.0 using the automated substitution model selection mode (PhyML-SMS) (*51*). Tree support for the ML analyses was assessed using an approximate likelihood-ratio test (aLRT) (*52*). In addition, standard bootstrap support for the ML trees was calculated in 100 replicates using PhyML v2.4.5, as implemented in the MacGDE package, based on the Whelan and Goldman (WAG) substitution model and taking into account among-site rate heterogeneity with four γ-distributed categories. The BI phylogenies were calculated using MrBayes implemented in the TOPALi v2.5 package (*53*). The BI analyses were based on the WAG substitution model taking into account the among-site rate heterogeneity with four γ-distributed categories. Posterior probability support values for the BI trees were calculated with two runs for 1,000,000 generations, with trees saved every 100 generations and with a 25% burn-in period.

Gene cloning

The genes encoding PduRAR and PduRXR were cloned from total RNA extracted from embryos at 48 or 75 hpf. The full-length receptors were subsequently tagged with a flag tag (DYKDDDDK) in the N-terminal domain of the receptor and cloned into the pSG5 vector. Chimeric GAL4 LBD receptors were created by cloning the LBD of the receptors into the pG4MpolyII vector that encodes the DNA binding domain of the Gal4 protein (that is, amino acids 1 to 147) (*54*). The PduRAR V356F mutant was constructed by replacing the valine in position 356 by a phenylalanine by polymerase chain reaction (PCR)–assisted, site-directed mutagenesis using the Pfu DNA polymerase (Promega). The Dpn I enzyme (New England Biolabs) was used to remove the parental DNA template.

Electrophoretic mobility shift assay

Genes encoding PduRAR and PduRXR cloned in pSG5 and containing a flag tag were used for EMSA experiments. Both receptors were translated in vitro and labeled with [^{35}S]methionine using the TNT wheat germ extract system (Promega), and assays were subsequently performed as previously described (*16*).

Ligands

The ligands ATRA, 9cRA, 13cRA, BMS493 (an RAR antagonist), BMS649 (an RXR agonist), and UVI3003 (an RXR antagonist) were purchased from Sigma-Aldrich. Stock solutions of the different compounds were prepared in ethanol at 10 mM.

Transactivation experiments

HEK 293T or COS (kidney from African green monkey) cells were maintained in Dulbecco's modified Eagle's medium (Invitrogen by Life Technologies), supplemented with 10% fetal calf serum (Invitrogen by Life Technologies). Transfections and treatments were performed as previously described (*20*) with 60 ng (for HEK 293T cells) or 400 ng (for COS cells) of total DNA, and the final concentrations of the different ligands were between 0.1 and 10 μM.

Limited proteolysis assay

Using the TNT coupled reticulocyte lysate system (Promega), the PduRAR receptor was translated and labeled with [^{35}S]methionine in vitro. LPA experiments were subsequently carried out as previously described (*16*), using final concentrations of the tested ligands between 0.1 and 10 μM.

Expression and purification of the PduRAR LBD

The wild-type PduRAR LBD was fused to His-thioredoxin, and the clone was subsequently transformed into BL21(DE3) *Escherichia coli* cells, which were grown at 37°C in LB medium supplemented with ampicillin (50 mg/ml) until the OD_{600} (optical density at 600 nm) reached about 0.6. The protein was overexpressed by addition of IPTG (isopropyl-β-D-thiogalactopyranoside) to a final concentration of 0.5 mM, and the culture was supplemented with 1 μM ATRA. After an

additional incubation for 8 hours at 18°C, the culture was harvested by centrifugation at 8000*g* for 20 min and stored at −80°C. Cell pellets from a total of 4 liters of culture were resuspended in 50 ml of buffer A [50 mM tris-HCl (pH 7.5), 500 mM NaCl, 1 mM dithiothreitol (DTT), 0.1 μM ATRA] supplemented with a protease inhibitor cocktail (cOmplete, Mini, EDTA-free) (Roche Applied Science). The suspension was lysed by sonication and centrifuged at 35,000*g* at 4°C for 45 min. The supernatant was loaded onto a nickel affinity column (5 ml; HisTrap) (GE Healthcare) preequilibrated with buffer A. The protein was eluted with buffer B [50 mM tris-HCl (pH 7.5), 500 mM NaCl, 1 mM DTT, 500 mM imidazole, 0.1 μM ATRA]. The fractions containing His-thioredoxin–PduRAR LBD–ATRA were pooled and treated with 1 mg of Tobacco Etch Virus (TEV) protease per 50 mg of PduRAR LBD and incubated at 16°C overnight. The digested proteins were then centrifuged at 15,000*g* for 20 min to remove TEV protease aggregates. The cleaved His-thioredoxin and PduRAR LBD–ATRA proteins were further separated by immobilized metal affinity chromatography, and the flow-through was subsequently concentrated to 20 mg/ml and purified by size exclusion chromatography (Superdex 75 HR 26/60) (GE Healthcare), which was preequilibrated with 20 mM tris (pH 7.5), 150 mM NaCl, 5 mM DTT, 1 mM EDTA, and 0.1 μM ATRA. The resulting protein complex was concentrated to 10 mg/ml.

Fluorescence anisotropy measurements

Fluorescence anisotropy assays were performed using a Safire 2 microplate reader (TECAN) with an excitation wavelength set at 470 nm and emission measured at 530 nm. The buffer solution for the assays was as follows: 20 mM tris-HCl (pH 7.5), 150 mM NaCl, 1 mM EDTA, 5 mM DTT, and 10% (v/v) glycerol. The measurements were initiated at the highest concentration of the PduRAR LBD (40 μM), and the protein sample was successively diluted twofold with a buffer solution. For each point of the titration curve, the protein sample was mixed with 4 nM fluorescent peptide and 30 μM ligand (final concentrations). Binding data were fitted using a sigmoidal dose-response model (GraphPad Prism, GraphPad Software), assuming the stoichiometry of one peptide per PduRAR LBD protein.

Structure determination and refinement

Crystals of the PduRAR LBD–ATRA complex were obtained in 0.2 M sodium acetate, 0.1 M Hepes (pH 7.5), and 20% polyethylene glycol 3000 by the hanging drop crystallization method. Single crystals were tested, and native data were collected from one crystal cryoprotected with 30% glycerol on the ID29 beam line at the European Synchrotron Radiation Facility in Grenoble, France. Data were analyzed for protein contaminants using ContaMiner (*55*). The crystal structure of the PduRAR LBD–ATRA complex was determined by molecular replacement using MoRDa (*56*). MoRDa placed four molecules in the asymmetric unit, forming two canonical nuclear receptor LBD dimers. However, the produced molecular replacement model was too poor for rebuilding and refinement, and molecular replacement phases were thus used for model rebuilding with phenix_build (*57*). The resulting model was refined using CCP4 ncsrefine (*58*), and the obtained phases were subjected to the Buccaneer software. The mtz output file was subsequently analyzed by Parrot, using fourfold noncrystallographic symmetry. In parallel, several homology models with different ligands and helix H12 positions were built using SWISS-MODEL. These models were superimposed on the Buccaneer Protein Data Bank (PDB) file and adjusted manually to the molecule with the best electron density (model B), using only the coot_rigid_body_fit_zone to the maps of the Parrot phases. The adjusted model was then used as a template and copied into the positions of the three other molecules in the asymmetric unit (molecules A, C, and D). Each new model was manually adjusted using coot_rigid_body_fit_zone. The Refmac program was used to refine this model (all B factors were set initially to 70 $Å^2$), using 20 steps of jelly body refinement. The Phenix software was used to obtain Translation/Libration/Screw (TLS) domains from this pdb file. These TLS domains were subsequently subjected to an analysis by the Lorestr program, and the resulting output was further refined in Refmac. The different input phases were tested by Buccaneer analyses on the final pdb, with the best results (as judged by R and R_{free} improvements) having been obtained by the Lorestr phases. Parrot was run on the Buccaneer mtz, and the resulting Parrot phases and the model from the final Refmac refinement were used as bases for manual adjustments and automated refinements with Refmac and Phenix.

Retinoid determination

Eggs, embryos, and adult tissues were stored at −80°C until assayed. Biological material was homogenized and subsequently extracted using a liquid-liquid extraction approach, as previously described (*4*). RA isomers were quantified using LC-MS/MS on an AB Sciex 5500 QTRAP in multistage-MRM (multiple reaction monitoring) mode using APCI (atmospheric pressure chemical ionization) in positive ion mode, as previously described (*4*, *25*). Retinol and retinyl esters were quantified by HPLC-UV on a Waters ACQUITY ultra-performance liquid chromatography system using a method that was previously described (*4*).

Detecting and imaging gene expression patterns

Gene expression patterns in *P. dumerilii* were assessed by whole-mount in situ hybridization, as previously described (*31*). After in situ hybridization, specimens were stained with DAPI (Invitrogen by Life Technologies) and immunohistochemically labeled with an acetylated α-tubulin antibody (Sigma-Aldrich) to visualize larval morphology and nervous system architecture (*31*). Developing *P. dumerilii* worms were subsequently imaged either as bright-field images with a Zeiss Axio Imager microscope and a Zeiss Axiocam MRc camera or as fluorescent images either by confocal reflection microscopy (*31*) with a Zeiss LD LCI Plan-Apochromat 25× 0.8 Oil/Glyc/Water DIC objective on a Zeiss LSM 780 NLO or by capturing the fluorescent spectra of the nitroblue tetrazolium/5-bromo-4-chloro-3-indolyl phosphate precipitate (*31*) with an Olympus UPLSAPO 60× 1.3 silicon objective on a spinning disc confocal system Olympus IX83 (excitation, 633 nm; reflector, 785/762 nm) with an Andor iXon 888 Ultra camera. To illustrate the complete expression patterns, *z* sections of bright-field images were merged with the software Helicon Focus. We used Adobe Photoshop CS5.1 and Adobe Illustrator CS5 to create the final figures.

Microinjection of *rar* and *rxr* MOs

We used MOs (Gene Tools LLC) to target the start codons of *P. dumerilii rar* (*rar* MO: AGTTGTCTTTGGAACATTTTCAAGT) and *rxr* (*rxr* MO: GATAACCTGCTACCCACTCCATCAC). Before ordering, the MO target regions were validated by comparing genomic contigs and transcriptomic data from *P. dumerilii* and by PCR on genomic DNA from different *P. dumerilii* specimens to ensure that the selected DNA stretches are free of single-nucleotide polymorphisms and are characterized by low overall polymorphism levels. As negative controls, a standard control MO (standard control MO: CCTCTTACCTCAGTTACAATTTATA) and 5-mismatch control MOs (*rar*-5mm control MO: AGTTcTCTTTcGAAgATTTTgAAcT and *rxr*-5mm control

MO: GATAACgTcCTAgCCAgTgCATCAC) were used. A 1 mM stock solution was prepared according to the manufacturer's instructions and subsequently filtered (0.22 μm). Unless otherwise indicated, a final MO concentration of 0.6 mM was used. The MOs were coinjected with a fluorescent tracer, either tetramethylrhodamine-dextran (Molecular Probes) or *h2b-rfp* mRNA, to visualize injected embryos. MOs were injected into the zygote on an inverted Zeiss Axiovert 40C microscope with self-pulled needles [borosilicate, thin wall with filament, 1.0 mm outside diameter (OD), 0.78 mm inside diameter (ID), 150 mm length (L)] (Harvard Apparatus) using a FemtoJet microinjector (Eppendorf) (settings: injection pressure, 300 hPa; injection pulse, 0.1 s; compensation pressure, 30 hPa). Needles were pulled on a Sutter Instrument P-97 Pipette Puller using the following settings: heat, 548; pull, 40; velocity, 130; time, 120; pressure, 500. Injections were carried out in a 16°C room, and injected embryos were cultured at 18°C. Developing *P. dumerilii* worms were subsequently fixed in 4% paraformaldehyde for further analysis. Specificity of the MOs was assessed in vivo. The MO target region was cloned upstream of a fluorescent tracer, *h2b-egfp*:pCS2+. The mRNA was transcribed in vitro using the mMESSAGE mMACHINE SP6 Transcription Kit (Life Technologies) and subsequently coinjected, at a final concentration of 200 ng/μl, with the corresponding MO (with or without mismatches) and with *h2b-rfp* mRNA, at a final concentration of 120 ng/μl, to visualize injected embryos.

Microinjection of *rar* mRNA

Full-length *P. dumerilii rar* was cloned either directly into pCS2+ or downstream of the fluorescent tracer Lyn-mCherry separated by a T2A self-cleaving peptide, resulting in two separate proteins upon translation. The fusion protein was inserted into pCS2+. The mRNAs were prepared as indicated above and injected at final concentrations of 220 to 400 ng/μl using the setup described above. The first *rar* mRNA was coinjectedwith a fluorescent tracer, tetramethylrhodamine-dextran (Molecular Probes), to visualize injected embryos. Embryos were fixed at 41 or 48 hpf in 4% paraformaldehyde and were subsequently immunostained. Before these experiments, we validated that the T2A peptide of the second mRNA construct is self-cleaving in *P. dumerilii* by injecting the mRNA of a fusion protein with two different fluorescent markers (Lyn-mCherry-T2A-H2B-GFP) into the *P. dumerilii* zygote.

Retinoid pharmacology

Developing *P. dumerilii* worms were treated with ATRA or 13cRA from 12 to 24 hpf, 34 to 40 hpf, 48 to 80 hpf, and 96 to 102 hpf. ATRA and 13cRA stock solutions (10 mM) were prepared in DMSO, aliquoted into amber tubes (Eppendorf), and stored at −80°C. The stock solution aliquots were defrosted and used only once. Drug treatments were performed in six-well plates in 6 ml of filtered (0.22 μm) natural seawater (NSW). NSW (3 ml) with 100 to 200 embryos was added to each well. The RA dilutions were prepared and mixed by vortexing in the remaining 3 ml of NSW before addition to the embryos. The final concentrations of the treatments were as follows: 1, 2, 4, 5, 8, and 10 μM. DMSO treatments were used as controls. After treatment, the six-well plate was covered with aluminum foil to avoid light exposure. Embryos were subsequently cultured at 18°C. At the end of the drug treatment, embryos were washed in NSW and fixed in 4% paraformaldehyde for further analysis. EdU labeling was performed before fixation and following the manufacturer's instructions (Invitrogen). The swimming behavior of *P. dumerilii* prelarvae and larvae, treated with ATRA or 13cRA, was recorded, respectively, with a Nikon Digital Sight DS-Fi1 camera and a DMK 42BUC03 camera (25 frames per second; The Imaging Source) and subsequently tracked with the Fiji plug-ins TrackMate (*59*) and MTrackJ (*60*).

SUPPLEMENTARY MATERIALS

Supplementary material for this article is available at http://advances.sciencemag.org/cgi/content/full/4/2/eaao1261/DC1

fig. S1. Phylogenetic analyses of the molecular components of retinoid metabolism and signaling in *P. dumerilii*.
fig. S2. Alignment of RAR sequences.
fig. S3. Transactivation assays using the PduRXR.
fig. S4. Structural analysis of the LBD of the PduRAR.
fig. S5. Expression of RA metabolic enzymes (*aldh1a* and *cyp26*) in *P. dumerilii*.
fig. S6. Validation of MOs for microinjection into *P. dumerilii* zygotes.
fig. S7. Effects of ATRA and 13cRA treatments on *P. dumerilii* larval development.
table S1. Data collection and refinement statistics for the PduRAR LBD–ATRA crystal structure complex.
movie S1. Locomotion of *P. dumerilii* larvae upon application of exogenous RA.
movie S2. Locomotion of *P. dumerilii* prelarvae upon application of exogenous RA.
References (*61*, *62*)

REFERENCES AND NOTES

1. K. Niederreither, P. Dollé, Retinoic acid in development: Towards an integrated view. *Nat. Rev. Genet.* **9**, 541–553 (2008).
2. T. J. Cunningham, G. Duester, Mechanisms of retinoic acid signalling and its roles in organ and limb development. *Nat. Rev. Mol. Cell Biol.* **16**, 110–123 (2015).
3. J. L. Napoli, Physiological insights into all-*trans*-retinoic acid biosynthesis. *Biochim. Biophys. Acta.* **1821**, 152–167 (2012).
4. M. A. Kane, J. L. Napoli, Quantification of endogenous retinoids. *Methods Mol. Biol.* **652**, 1–54 (2010).
5. P. Chambon, A decade of molecular biology of retinoic acid receptors. *FASEB J.* **10**, 940–954 (1996).
6. J. E. Balmer, R. Blomhoff, A robust characterization of retinoic acid response elements based on a comparison of sites in three species. *J. Steroid Biochem. Mol. Biol.* **96**, 347–354 (2005).
7. A. Chatagnon, P. Veber, V. Morin, J. Bedo, G. Triqueneaux, M. Sémon, V. Laudet, F. d'Alché-Buc, G. Benoit, RAR/RXR binding dynamics distinguish pluripotency from differentiation associated cis-regulatory elements. *Nucleic Acids Res.* **43**, 4833–4854 (2015).
8. P. Germain, P. Chambon, G. Eichele, R. M. Evans, M. A. Lazar, M. Leid, A. R. De Lera, R. Lotan, D. J. Mangelsdorf, H. Gronemeyer, International Union of Pharmacology. LX. Retinoic acid receptors. *Pharmacol. Rev.* **58**, 712–725 (2006).
9. H. Gronemeyer, J.-Å. Gustafsson, V. Laudet, Principles for modulation of the nuclear receptor superfamily. *Nat. Rev. Drug Discov.* **3**, 950–964 (2004).
10. M. A. Mendoza-Parra, M. Walia, M. Sankar, H. Gronemeyer, Dissecting the retinoid-induced differentiation of F9 embryonal stem cells by integrative genomics. *Mol. Syst. Biol.* **7**, 538 (2011).
11. E. Moutier, T. Ye, M.-A. Choukrallah, S. Urban, J. Osz, A. Chatagnon, L. Delacroix, D. Langer, N. Rochel, D. Moras, G. Benoit, I. Davidson, Retinoic acid receptors recognize the mouse genome through binding elements with diverse spacing and topology. *J. Biol. Chem.* **287**, 26328–26341 (2012).
12. F. Campo-Paysaa, F. Marlétaz, V. Laudet, M. Schubert, Retinoic acid signaling in development: Tissue-specific functions and evolutionary origins. *Genesis* **46**, 640–656 (2008).
13. R. Albalat, C. Cañestro, Identification of Aldh1a, Cyp26 and RAR orthologs in protostomes pushes back the retinoic acid genetic machinery in evolutionary time to the bilaterian ancestor. *Chem. Biol. Interact.* **178**, 188–196 (2009).
14. N. I. Bakalenko, A. V. Poznyak, E. L. Novikova, M. A. Kulakova, Effect of retinoids on *Post2 Hox* gene expression in nereid polychaetes. *Russ. J. Dev. Biol.* **48**, 211–218 (2017).
15. H. Urushitani, Y. Katsu, Y. Ohta, H. Shiraishi, T. Iguchi, T. Horiguchi, Cloning and characterization of the retinoic acid receptor-like protein in the rock shell, *Thais clavigera*. *Aquat. Toxicol.* **142–143**, 403–413 (2013).
16. J. Gutierrez-Mazariegos, E. K. Nadendla, D. Lima, K. Pierzchalski, J. W. Jones, M. Kane, J.-I. Nishikawa, Y. Hiromori, T. Nakanishi, M. M. Santos, L. F. C. Castro, W. Bourguet, M. Schubert, V. Laudet, A mollusk retinoic acid receptor (RAR) ortholog sheds light on the evolution of ligand binding. *Endocrinology* **155**, 4275–4286 (2014).
17. A. H. L. Fischer, T. Henrich, D. Arendt, The normal development of *Platynereis dumerilii* (Nereididae, Annelida). *Front. Zool.* **7**, 31 (2010).

18. R. Albalat, F. Brunet, V. Laudet, M. Schubert, Evolution of retinoid and steroid signaling: Vertebrate diversification from an amphioxus perspective. *Genome Biol. Evol.* **3**, 985–1005 (2011).
19. J.-P. Renaud, N. Rochel, M. Ruff, V. Vivat, P. Chambon, H. Gronemeyer, D. Moras, Crystal structure of the RAR-γ ligand-binding domain bound to all-*trans* retinoic acid. *Nature* **378**, 681–689 (1995).
20. H. Escriva, S. Bertrand, P. Germain, M. Robinson-Rechavi, M. Umbhauer, J. Cartry, M. Duffraisse, L. Holland, H. Gronemeyer, V. Laudet, Neofunctionalization in vertebrates: The example of retinoic acid receptors. *PLOS Genet.* **2**, e102 (2006).
21. P. Germain, J. Iyer, C. Zechel, H. Gronemeyer, Co-regulator recruitment and the mechanism of retinoic acid receptor synergy. *Nature* **415**, 187–192 (2002).
22. P. F. Egea, A. Mitschler, D. Moras, Molecular recognition of agonist ligands by RXRs. *Mol. Endocrinol.* **16**, 987–997 (2002).
23. V. Nahoum, E. Pérez, P. Germain, F. Rodríguez-Barrios, F. Manzo, S. Kammerer, G. Lemaire, O. Hirsch, C. A. Royer, H. Gronemeyer, A. R. de Lera, W. Bourguet, Modulators of the structural dynamics of the retinoid X receptor to reveal receptor function. *Proc. Natl. Acad. Sci. U.S.A.* **104**, 17323–17328 (2007).
24. A. le Maire, C. Teyssier, C. Erb, M. Grimaldi, S. Alvarez, A. R. de Lera, P. Balaguer, H. Gronemeyer, C. A. Royer, P. Germain, W. Bourguet, A unique secondary-structure switch controls constitutive gene repression by retinoic acid receptor. *Nat. Struct. Mol. Biol.* **17**, 801–807 (2010).
25. J. W. Jones, K. Pierzchalski, J. Yu, M. A. Kane, Use of fast HPLC multiple reaction monitoring cubed for endogenous retinoic acid quantification in complex matrices. *Anal. Chem.* **87**, 3222–3230 (2015).
26. M. A. Kane, Analysis, occurrence, and function of 9-cis-retinoic acid. *Biochim. Biophys. Acta* **1821**, 10–20 (2012).
27. R. Blomhoff, H. K. Blomhoff, Overview of retinoid metabolism and function. *Dev. Neurobiol.* **66**, 606–630 (2006).
28. G. Begemann, T. F. Schilling, G.-J. Rauch, R. Geisler, P. W. Ingham, The zebrafish *neckless* mutation reveals a requirement for *raldh2* in mesodermal signals that pattern the hindbrain. *Development* **128**, 3081–3094 (2001).
29. A. S. Denes, G. Jékely, P. R. H. Steinmetz, F. Raible, H. Snyman, B. Prud'homme, D. E. K. Ferrier, G. Balavoine, D. Arendt, Molecular architecture of annelid nerve cord supports common origin of nervous system centralization in Bilateria. *Cell* **129**, 277–288 (2007).
30. J. N. Rosen, M. F. Sweeney, J. D. Mably, Microinjection of zebrafish embryos to analyze gene function. *J. Vis. Exp.* e1115 (2009).
31. G. Jékely, D. Arendt, Cellular resolution expression profiling using confocal detection of NBT/BCIP precipitate by reflection microscopy. *Biotechniques* **42**, 751–755 (2007).
32. S. Arber, B. Han, M. Mendelsohn, M. Smith, T. M. Jessell, S. Sockanathan, Requirement for the homeobox gene *Hb9* in the consolidation of motor neuron identity. *Neuron* **23**, 659–674 (1999).
33. M. Kulakova, N. Bakalenko, E. Novikova, C. E. Cook, E. Eliseeva, P. R. H. Steinmetz, R. P. Kostyuchenko, A. Dondua, D. Arendt, M. Akam, T. Andreeva, Hox gene expression in larval development of the polychaetes *Nereis virens* and *Platynereis dumerilii* (Annelida, Lophotrochozoa). *Dev. Genes Evol.* **217**, 39–54 (2007).
34. J. Gutierrez-Mazariegos, "Evolution of the retinoic acid receptor," thesis, Ecole Normale Supérieure de Lyon (2014).
35. S. G. Mansfield, S. Cammer, S. C. Alexander, D. P. Muehleisen, R. S. Gray, A. Tropsha, W. E. Bollenbacher, Molecular cloning and characterization of an invertebrate cellular retinoic acid binding protein. *Proc. Natl. Acad. Sci. U.S.A.* **95**, 6825–6830 (1998).
36. I. Söderhäll, A. Tangprasittipap, H. Liu, K. Sritunyalucksana, P. Prasertsan, P. Jiravanichpaisal, K. Söderhäll, Characterization of a hemocyte intracellular fatty acid-binding protein from crayfish (*Pacifastacus leniusculus*) and shrimp (*Penaeus monodon*). *FEBS J.* **273**, 2902–2912 (2006).
37. R. J. White, Q. Nie, A. D. Lander, T. F. Schilling, Complex regulation of *cyp26a1* creates a robust retinoic acid gradient in the zebrafish embryo. *PLOS Biol.* **5**, e304 (2007).
38. Z. Kostrouch, M. Kostrouchova, W. Love, E. Jannini, J. Piatigorsky, J. E. Rall, Retinoic acid X receptor in the diploblast, *Tripedalia cystophora*. *Proc. Natl. Acad. Sci. U.S.A.* **95**, 13442–13447 (1998).
39. B. Fuchs, W. Wang, S. Graspeuntner, Y. Li, S. Insua, E.-M. Herbst, P. Dirksen, A.-M. Böhm, G. Hemmrich, F. Sommer, T. Domazet-Lošo, U. C. Klostermeier, F. Anton-Erxleben, P. Rosenstiel, T. C. G. Bosch, K. Khalturin, Regulation of polyp-to-jellyfish transition in *Aurelia aurita*. *Curr. Biol.* **24**, 263–273 (2014).
40. M. Bouzaiene, A. Angers, M. Anctil, Immunohistochemical localization of a retinoic acid-like receptor in nerve cells of two colonial anthozoans (Cnidaria). *Tissue Cell* **39**, 123–130 (2007).
41. D. Estephane, M. Anctil, Retinoic acid and nitric oxide promote cell proliferation and differentially induce neuronal differentiation *in vitro* in the cnidarian *Renilla koellikeri*. *Dev. Neurobiol.* **70**, 842–852 (2010).
42. R. Pennati, A. Dell'Anna, G. Zega, F. De Bernardi, S. Piraino, Retinoic acid influences antero-posterior positioning of peptidergic neurons in the planula larva of the hydrozoan *Clava multicornis*. *Mar. Ecol.* **34**, 143–152 (2013).
43. C. J. Carter, N. Farrar, R. L. Carlone, G. E. Spencer, Developmental expression of a molluscan RXR and evidence for its novel, nongenomic role in growth cone guidance. *Dev. Biol.* **343**, 124–137 (2010).
44. M. Maden, G. Keen, G. E. Jones, Retinoic acid as a chemotactic molecule in neuronal development. *Int. J. Dev. Neurosci.* **16**, 317–322 (1998).
45. J. M. Dmetrichuk, G. E. Spencer, R. L. Carlone, Retinoic acid-dependent attraction of adult spinal cord axons towards regenerating newt limb blastemas *in vitro*. *Dev. Biol.* **281**, 112–120 (2005).
46. A. Janesick, S. C. Wu, B. Blumberg, Retinoic acid signaling and neuronal differentiation. *Cell. Mol. Life Sci.* **72**, 1559–1576 (2015).
47. A. Linville, K. Radtke, J. S. Waxman, D. Yelon, T. F. Schilling, Combinatorial roles for zebrafish retinoic acid receptors in the hindbrain, limbs and pharyngeal arches. *Dev. Biol.* **325**, 60–70 (2009).
48. J. S. Dasen, T. M. Jessell, Hox networks and the origins of motor neuron diversity. *Curr. Top. Dev. Biol.* **88**, 169–200 (2009).
49. M. Conzelmann, E. A. Williams, K. Krug, M. Franz-Wachtel, B. Macek, G. Jékely, The neuropeptide complement of the marine annelid *Platynereis dumerilii*. *BMC Genomics* **14**, 906 (2013).
50. R. C. Edgar, MUSCLE: Multiple sequence alignment with high accuracy and high throughput. *Nucleic Acids Res.* **32**, 1792–1797 (2004).
51. S. Guindon, J.-F. Dufayard, V. Lefort, M. Anisimova, W. Hordijk, O. Gascuel, New algorithms and methods to estimate maximum-likelihood phylogenies: Assessing the performance of PhyML 3.0. *Syst. Biol.* **59**, 307–321 (2010).
52. M. Anisimova, O. Gascuel, Approximate likelihood-ratio test for branches: A fast, accurate, and powerful alternative. *Syst. Biol.* **55**, 539–552 (2006).
53. I. Milne, F. Wright, G. Rowe, D. F. Marshall, D. Husmeier, G. McGuire, TOPALi: Software for automatic identification of recombinant sequences within DNA multiple alignments. *Bioinformatics* **20**, 1806–1807 (2004).
54. G. Allenby, M. T. Bocquel, M. Saunders, S. Kazmer, J. Speck, M. Rosenberger, A. Lovey, P. Kastner, J. F. Grippo, P. Chambon, Retinoic acid receptors and retinoid X receptors: Interactions with endogenous retinoic acids. *Proc. Natl. Acad. Sci. U.S.A.* **90**, 30–34 (1993).
55. A. Hungler, A. Momin, K. Diederichs, S. T. Arold, *ContaMiner* and ContaBase: A webserver and database for early identification of unwantedly crystallized protein contaminants. *J. Appl. Crystallogr.* **49**, 2252–2258 (2016).
56. A. Vagin, A. Lebedev, MoRDa, an automatic molecular replacement pipeline. *Acta Crystallogr. A* **71**, s19 (2015).
57. P. D. Adams, D. Baker, A. T. Brunger, R. Das, F. DiMaio, R. J. Read, D. C. Richardson, J. S. Richardson, T. C. Terwilliger, Advances, interactions, and future developments in the CNS, Phenix, and Rosetta structural biology software systems. *Annu. Rev. Biophys.* **42**, 265–287 (2013).
58. Collaborative Computational Project, Number 4, The *CCP*4 suite: Programs for protein crystallography. *Acta Crystallogr. D Biol. Crystallogr.* **50**, 760–763 (1994).
59. J.-Y. Tinevez, N. Perry, J. Schindelin, G. M. Hoopes, G. D. Reynolds, E. Laplantine, S. Y. Bednarek, S. L. Shorte, K. W. Eliceiri, TrackMate: An open and extensible platform for single-particle tracking. *Methods* **115**, 80–90 (2017).
60. E. Meijering, O. Dzyubachyk, I. Smal, Methods for cell and particle tracking. *Methods Enzymol.* **504**, 183–200 (2012).
61. M. Gouy, S. Guindon, O. Gascuel, SeaView version 4: A multiplatform graphical user interface for sequence alignment and phylogenetic tree building. *Mol. Biol. Evol.* **27**, 221–224 (2010).
62. M. Kearse, R. Moir, A. Wilson, S. Stones-Havas, M. Cheung, S. Sturrock, S. Buxton, A. Cooper, S. Markowitz, C. Duran, T. Thierer, B. Ashton, P. Meintjes, A. Drummond, Geneious Basic: An integrated and extendable desktop software platform for the organization and analysis of sequence data. *Bioinformatics* **28**, 1647–1649 (2012).

Acknowledgments: We are indebted to N. Robert, M. Sémon, O. Simakov, and T. Larsson for help with bioinformatic analyses. K. Achim, P. Mejstrik, and G. Holzer supported pharmacological treatments, whole-mount in situ hybridization experiments, and transactivation assays, respectively. We also thank S. P. Singh for providing plasmids and K. Skouloudaki for discussions. **Funding:** This work was financed by the European Molecular Biology Laboratory (to M.H.-T., P.Y.B., and D.A.), the Ministerio de Ciencia e Innovación (ES-2008-236 to M.H.-T. and BFU2010-14875 to R.A.), the European Research Council (HOURGLASS no. 260746 to M.H.-T. and P.T. and BrainEvoDevo no. 294810 to P.Y.B. and D.A.), the King Abdullah University of Science and Technology (to S.T.A.), the Ministerio de Economía y Competitividad (BIO2015-67358-C2-1-P to R.A.), the French Infrastructure for Integrated Structural Biology program (ANR-10-INBS-05 to W.B.), and the Agence Nationale de la Recherche (ANR-11-JSV2-002-01 to M.S.). **Author contributions:** M.H.-T. and J.G.-M. screened sequence databases for *P. dumerilii* genes, which were cloned by M.H.-T. J.G.-M. and P.G. performed in vitro studies. S.T.A., E.K.N., and W.B. obtained the PduRAR crystal and solved the

crystal structure. S.T.A., P.G., and W.B. refined and analyzed the crystal structure. R.A. performed phylogenetic calculations, with support from M.H.-T., J.G.-M., and M.S. K.P., J.W.J., and M.A.K. carried out retinoid content analyses on material collected by M.H.-T. and J.G.-M. M.H.-T. performed microinjections and, together with P.Y.B., pharmacological treatments. M.H.-T., P.Y.B., and P.T. carried out whole-mount in situ hybridization and immunohistochemistry experiments. M.H.-T., J.G.-M., V.L., D.A., and M.S. designed the study and analyzed data. M.H.-T., V.L., D.A., and M.S. wrote the manuscript. M.H.-T. and M.S. finalized figures, tables, and text. All authors commented on the manuscript and agreed to its final version. **Competing interests:** The authors declare that they have no competing interests. **Data and material availability:** All data needed to evaluate the conclusions in this study are presented in the paper and/or the Supplementary Materials. Additional data related to this paper may be requested from the authors. The *P. dumerilii* sequences have been deposited in the GenBank nucleotide database with accession numbers KY679090 to KY679137. The PduRAR crystal structure has been submitted to the PDB archive, with the PDB ID 6EU9.

Submitted 19 June 2017
Accepted 10 January 2018
Published 21 February 2018
10.1126/sciadv.aao1261

Citation: M. Handberg-Thorsager, J. Gutierrez-Mazariegos, S. T. Arold, E. Kumar Nadendla, P. Y. Bertucci, P. Germain, P. Tomançak, K. Pierzchalski, J. W. Jones, R. Albalat, M. A. Kane, W. Bourguet, V. Laudet, D. Arendt, M. Schubert, The ancestral retinoic acid receptor was a low-affinity sensor triggering neuronal differentiation. *Sci. Adv.* **4**, eaao1261 (2018).

The ancestral retinoic acid receptor was a low-affinity sensor triggering neuronal differentiation

Mette Handberg-Thorsager, Juliana Gutierrez-Mazariegos, Stefan T. Arold, Eswar Kumar Nadendla, Paola Y. Bertucci, Pierre Germain, Pavel Tomançak, Keely Pierzchalski, Jace W. Jones, Ricard Albalat, Maureen A. Kane, William Bourguet, Vincent Laudet, Detlev Arendt and Michael Schubert

Sci Adv **4** (2), eaao1261.
DOI: 10.1126/sciadv.aao1261